



Threshold indicators of primary production in the north-east Atlantic for assessing environmental disturbances using 21 years of satellite ocean colour



Gavin H. Tilstone^{a,*}, Peter E. Land^a, Silvia Pardo^a, Onur Kerimoglu^b, Dimitry Van der Zande^c

^a Plymouth Marine Laboratory, Prospect Place, West Hoe, Plymouth PL1 3DH, UK

^b Institute for Chemistry and Biology of the Marine Environment, University of Oldenburg, Oldenburg, Germany

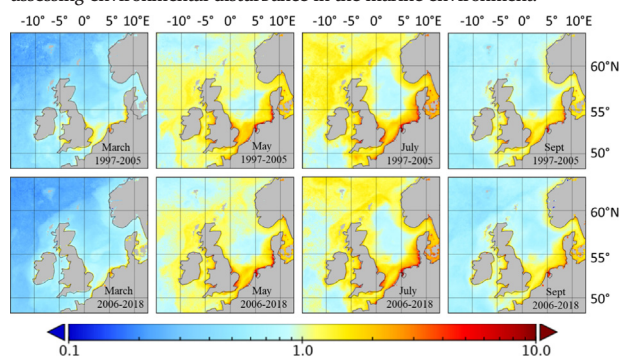
^c Royal Belgian Institute of Natural Sciences, 29 Rue Vautier, 1000 Brussels, Belgium

HIGHLIGHTS

- **OBJECTIVE** Chlorophyll-*a* has previously been used as an indicator of water quality.
- **ADDRESSING the PROBLEM** Primary production (PP) is a better indicator of marine environment disturbance.
- **MAJOR METHOD** Satellite PP is used to define threshold values to detect environmental disturbance.
- **MAJOR FINDING** Threshold values detect Eyjafjallajökull volcano and river nutrient run-off effects.
- **TAKE HOME MESSAGE** This is an accurate way of detecting anthropogenic effects in the marine environment.

GRAPHICAL ABSTRACT

Mean monthly primary production 90th percentile (gC m⁻² d⁻¹) for March, May, July and September using CMEMS Ocean Colour data from 1997-2005 and 2006-2018 for the north-east Atlantic and North West European Shelf for assessing environmental disturbance in the marine environment.



ARTICLE INFO

Editor: Martin Drews

Keywords:

Phytoplankton
Primary production
North-East Atlantic
Baseline
Thresholds
Time series
Climatology
Phenology
90th percentile

ABSTRACT

Primary production (PP) is highly sensitive to changes in the ecosystem and can be used as an early warning indicator for disturbance in the marine environment. Historic indicators of good environmental status of the north-east (NE) Atlantic and north-west (NW) European Seas suggested that daily PP should not exceed 2–3 g C m⁻² d⁻¹ during phytoplankton blooms and that annual rates should be <300 g C m⁻² yr⁻¹. We use 21 years of Copernicus Marine Service (CMEMS) Ocean Colour data from September 1997 to December 2018 to assess areas in the NE Atlantic with similar peak, climatology, phenology and annual PP values. Daily and annual thresholds of the 90th percentile (P90) of PP are defined for these areas and PP values above these thresholds indicate disturbances, both natural and anthropogenic, in the marine environment. Two case studies are used to test the validity and accuracy of these thresholds. The first is the eruption of the volcano Eyjafjallajökull, which deposited large volumes of volcanic dust (and therefore iron) into the NE Atlantic during April and May 2010. A clear signature in both PP and chlorophyll-*a* (Chl *a*) was evident from 28th April to 6th May and from 18th to 27th May 2010, when PP exceeded the PP P90 threshold for the region, which was comparatively more sensitive than Chl *a* P90 as an indicator of this disturbance. The second case study was for the riverine input of total nitrogen and phosphorus, along the Wadden Sea coast in the North Sea. During years when total nitrogen and phosphorus were above the climatology maximum, there was a lag signature in both PP and Chl *a* when PP exceeded the PP P90 threshold defined for the study area which was slightly more sensitive than Chl *a* P90. This technique represents an accurate means of determining disturbances in the environment both in the coastal and offshore waters in the NE Atlantic using remotely sensed ocean colour data.

* Corresponding author.

E-mail address: ghti@pml.ac.uk (G.H. Tilstone).

1. Introduction

Phytoplankton are responsible for about half of global primary production (PP) (Longhurst et al., 1995) and in the North (N) Atlantic, represent a significant sink for CO₂ (Takahashi et al., 2009). PP is driven by light, nutrients (both macro- and micro-nutrients, such as iron) and temperature (Koertinger et al., 2008). Any perturbations in these parameters, be it from natural disturbances such as volcanic activity, dust deposition, wildfires, or anthropogenic disturbances such as climate change and eutrophication, can be reflected in the magnitude and timing of daily PP, which ultimately affect the annual rates of PP. Understanding the variation in Chl *a* and PP under the influence of the natural range of water column mixing, light and nutrient regimes is necessary to distinguish the natural seasonal cycle from environmental perturbations caused by anthropogenic and natural disturbances that are outside of this envelope. Increases in Chl *a* and PP are often associated with increases in fish stocks (Marshak and Link, 2021), but this depends on the dominant species present in the phytoplankton community and the timing and synchronisation with zooplankton. Disturbances in the environment such as hydrological changes, contaminants, nutrient inputs or climate change, may not necessarily be detected through changes in Chl *a* alone, but can be identified through changes in phytoplankton photosynthetic rates and PP (Boalch, 1987), though this has not yet been verified. The flow of carbon between phytoplankton productivity and higher trophic levels means that PP can potentially be used as an early warning for direct pressure on food webs. Increases in Chl *a* and PP also lead to an accumulation of organic matter (Nixon, 1995), which in turn can stimulate bacterial activity, resulting in undesirable changes in aquatic chemistry and a degradation of water quality (Cloern, 2001; Rabalais et al., 2009). PP may also be a better indicator of bacterial production, and water quality in general, for the marine environment compared to Chl *a*.

Anthropogenic disturbances in coastal regions of the north-east Atlantic due to an increase in nitrogen through river run-off were widely reported during the 1950's to 1970's (Lehmusluoto and Pesonen, 1973; Ryther and Dunstan, 1971), which increased phytoplankton PP and hypoxia, and changed the phytoplankton species composition. In the Irish Sea, total organic nitrogen concentrations increased from 5 to 8 μmol L⁻¹, which caused a significant rise in phytoplankton biomass and production (Allen et al., 1998). In northern European coastal regions in particular, this led to a disruption in the balance between the production and the turnover of organic matter (Cloern, 2001). During the 1980s, the North Sea also experienced abrupt increases in both Sea Surface Temperature (SST) and PP (Beaugrand, 2004; Reid et al., 2001a; Reid et al., 2001b), and an increase in the occurrence of dinoflagellate-dominated harmful algal blooms (Hallegraeff, 2010).

As part of an international effort to ensure that we have clean and sustainable seas into the future, many national and cross-border threshold or indicator levels have been established. In Europe, the EU Marine Strategy Framework Directive (MSFD) uses 11 key descriptor parameters to measure “good environmental status” (GES) to ensure that the marine environment is safeguarded for future generations (Commission, 2008). For phytoplankton, three metrics that assess ecological status are used: phytoplankton biomass (or Chl *a*), phytoplankton composition and abundance, and phytoplankton bloom intensity and frequency (Brito et al., 2012; Devlin et al., 2007). A threshold of peak biomass defined as Chl *a* P90 has been widely used as an operational indicator for the assessment of ecological status and water quality (OSPAR, 2017). The practical implementation of thresholds in these parameters provides a tool to assess whether pollution is reduced sufficiently, especially from urban and agricultural sources, so that water bodies are in GES and hence, the marine environment is preserved. These include Chl *a* and an initial target to meet these was set for 2020 (Commission, 2000, 2008; OSPAR, 2017). Monitoring these key descriptors over large maritime areas poses a logistical and economic challenge for ship-borne surveys and obtaining sufficient *in situ* data, both spatially and temporally, to assess whether these thresholds are exceeded, remains a challenge (Chang et al., 2015). Some of the GES descriptor

parameters are available from satellite that can provide enhanced spatial and temporal data coverage. With the advent of ocean colour and the increase in the number, accuracy and resolution of satellite sensors, these data are increasingly being used to track anthropogenic disturbances in the marine environment (Cristina et al., 2015; Novoa et al., 2012). There is on-going effort to integrate *in situ* with satellite data to re-determine baselines and indicator thresholds for certain regions (Garcia-Garcia et al., 2019). This has proved successful in countries that have large maritime areas with extensive exclusive economic zones (Cristina et al., 2015). A candidate parameter for the MSFD is time series of PP. During the 1970's and 1980's, using two decades of PP data collected from the western English Channel, baseline thresholds were determined and defined as 2–3 g C m⁻² d⁻¹ during phytoplankton blooms and that annual rates should not exceed 300 g C m⁻² yr⁻¹ (Boalch, 1987; Boalch et al., 1978). PP and Chl *a* thresholds need to be compared to assess whether they react similarly to environmental disturbances, what causes any potential differences between them and whether one of the metrics is more sensitive.

The objectives of this paper are to assess regions of similar peak and timing of PP in the NE Atlantic and from these, to define baseline threshold values of PP based on its 90th percentile (P90) over a reference period for each region for use in detecting disturbances in the marine environment. Similar thresholds of Chl *a* can also be defined. Once thresholds of PP and Chl *a* are defined, they are then used to evaluate disturbances in the marine environment using two case studies to determine whether the PP P90 and Chl *a* P90 thresholds are appropriate. The first case study is the eruption of the Eyjafjallajökull volcano in 2010, which deposited large quantities of iron into the north-east Atlantic (Achterberg et al., 2013). The second is the anthropogenic input of high nutrient loads into the North Sea along the Wadden Sea coast.

2. Material and methods

2.1. Study area

The study area is the NE Atlantic encompassing the Celtic, Irish and North Seas from 48 to 60°N, 15°W to 10°E.

2.2. Remote sensing data

2.2.1. Copernicus marine environment monitoring service (CMEMS) ocean colour data

Daily CMEMS Chl-*a* (mg m⁻³) images at 0.05° resolution (OCEANCOLOUR_ATL_BGC_L3_MY_009_067) were used to model PP. The data are derived from the European Space Agency Ocean Colour Climate Change Initiative (OC-CCI) remote sensing reflectance (R_{rs}) data using the OC5CI Chl *a* algorithm (Sathyendranath et al., 2019). The data cover the period from September 1997 to December 2018, and include merged ocean colour data from SeaWiFS, MODIS-Aqua, MERIS and VIIRS missions. The OC5CI algorithm is a switching algorithm that applies the OC5 model (Gohin, 2011) in Case 2 coastal regions and the colour index (Hu et al., 2012) in Case 1 open ocean areas. OC5 is a version of the widely used OC4, modified to include an empirical parameterisation of 412 and 560 nm channels related to the absorption of CDOM and scattering of SPM (Novoa et al., 2012; Saulquin et al., 2011). The Chl *a* concentration is determined from the triplet values of OC4 maximum normalised water leaving radiance (nL_w) band ratio, $nL_w(412)$ and $nL_w(560)$, from a Look Up Table (LUT), based on the relationships between measured Chl *a* and satellite $R_{rs}(\lambda)$ from observations in the English Channel and Bay of Biscay (Gohin et al., 2002). OC5 has a proven legacy of performing best when compared to a number of other coastal Chl *a* algorithms when applied to a range of ocean colour sensors (Lapucci et al., 2012; Loisel et al., 2017; Novoa et al., 2012; Tilstone et al., 2011). In NW European waters, OC5 has an accuracy of 25 % compared to *in situ* Chl *a* (Tilstone et al., 2017). The CI algorithm was developed for open-ocean low Chl *a* waters (Hu et al., 2012) and has proven to be accurate using an array of different ocean colour sensors (Tilstone et al., 2021).

2.2.2. Primary production

A wavelength resolving model (WRM) of PP (Morel, 1991) was implemented following Smyth et al. (2005) using daily 0.05° CMEMS OC5CI Chl *a*, SeaWiFS and MODIS photosynthetically available radiation (PAR, <https://oceandata.sci.gsfc.nasa.gov/directaccess/>) and the CMEMS global SST product (SST_GLO_SST_L4_REP_OBSERVATIONS_010_011) to generate mean monthly satellite maps of PP from 1997 to 2018 (Fig. 1). The accuracy of this satellite PP model is well documented (Antoine et al., 1996; Tilstone et al., 2009; Tilstone et al., 2005; Tilstone et al., 2015). Over the past two decades NASA undertook three round-robin PP inter-comparisons, which also characterised the sources of error associated with the algorithms (Carr et al., 2006; Friedrichs et al., 2009; Saba et al., 2011). The WRM model of Smyth et al. (2005) was entered in all of the inter-comparisons, the most comprehensive of which was Saba et al. (2011), who compared 36 models of primary production against a large *in situ* dataset of PP measured using ^{14}C ($N = 1156$). The average uncertainty across all models was 31 % and the Smyth et al. (2005) model proved to be one of the most accurate in eight out of ten regions. Similarly, Tilstone et al. (2009) compared three commonly used PP models in the Atlantic Ocean and found that a WRM was the most accurate in six out of nine Atlantic Ocean biogeographic provinces and was within 30 % of *in situ* ^{14}C PP.

2.2.3. Case 2 water type mask

Optically complex 'case 2' coastal waters (Morel and Prieur, 1977) pose many challenges for the accurate determination of satellite ocean colour Chl *a* concentrations due to non-covarying concentrations of suspended particulate matter (SPM) and coloured dissolved organic matter (CDOM). While the OC5 algorithm is capable of providing good Chl *a* estimates in clear offshore waters (*i.e.* Case 1 waters) and moderately turbid coastal waters (Gohin et al., 2008), there is a limit to its applicability where the algorithm is expected to overestimate Chl *a* in extremely turbid waters (Novoa et al., 2012) and underestimate Chl *a* in hyper-eutrophic waters (Tilstone et al., 2017). In addition to the effect on Chl *a* retrieval, Case 2 waters can also affect the calculation of PP through the effects of SPM and CDOM on the in-water light field. The effect of SPM is second order, since the reduction in light penetration through the water column due to SPM scattering is

offset by the resulting increase in PAR in the remaining photic zone and it is not included in the PP model (Smyth et al., 2005). CDOM absorption similarly reduces light penetration, but with no offset increase in PAR. The PP model either accounts for CDOM directly if CDOM measurements are available, or by assuming CDOM to be autochthonous and relating it to the Chl *a* concentration. The PP used in this study is calculated using the latter assumption, so as well as needing to mask high CDOM because of its effect on the Chl *a* algorithm, it is important to mask CDOM values significantly higher than expected from Chl *a*, because they will cause overestimation of PP even if the Chl *a* retrieval is accurate.

Lavigne et al. (2021) quantified the limits of applicability as thresholds of $R_{rs}(560) / R_{rs}(490)$ (used as a proxy for high Chl *a*), $R_{rs}(560)$ (proxy for high SPM) and $R_{rs}(412) / R_{rs}(443)$ (proxy for high CDOM), allowing for the application of a pixel-based quality control procedure to flag out pixels where the OC5 algorithm and/or the PP model is expected to perform poorly. Using a dataset of 348 *in situ* Chl *a* and satellite matchups, it was shown that by removing flagged data, the performance of the Chl *a* algorithm is significantly improved resulting in median absolute percent difference errors of approximately 30 % (Lavigne et al., 2021). The quality control procedure was applied to the daily CMEMS Chl *a* products used in this study and hence to PP, which is calculated from Chl *a*.

2.3. Statistical methods

K-means clustering based on peak and timing of satellite PP was used to identify regions of similarity. At each location, the daily climatological mean PP over a reference period of over eight years (September 1997 to December 2005) was used to calculate maximum PP, the day number at which it occurs and the annual PP. These together with latitude and longitude were normalised to zero mean and unit standard deviation and used as parameters in K-means cluster analysis to define *N* regions with similar characteristics. The region boundaries were then sharpened using two measures. The first considers the distance of each location from the eight class centres in normalised parameter space. The distance d_i from each region is then compared with the minimum distance to all other regions d_{\min} to obtain a proximity measure $p_{1i} = d_{\min} / (d_i + d_{\min})$. The second counts the number (n_i) of the eight pixels neighbouring each location that belong to

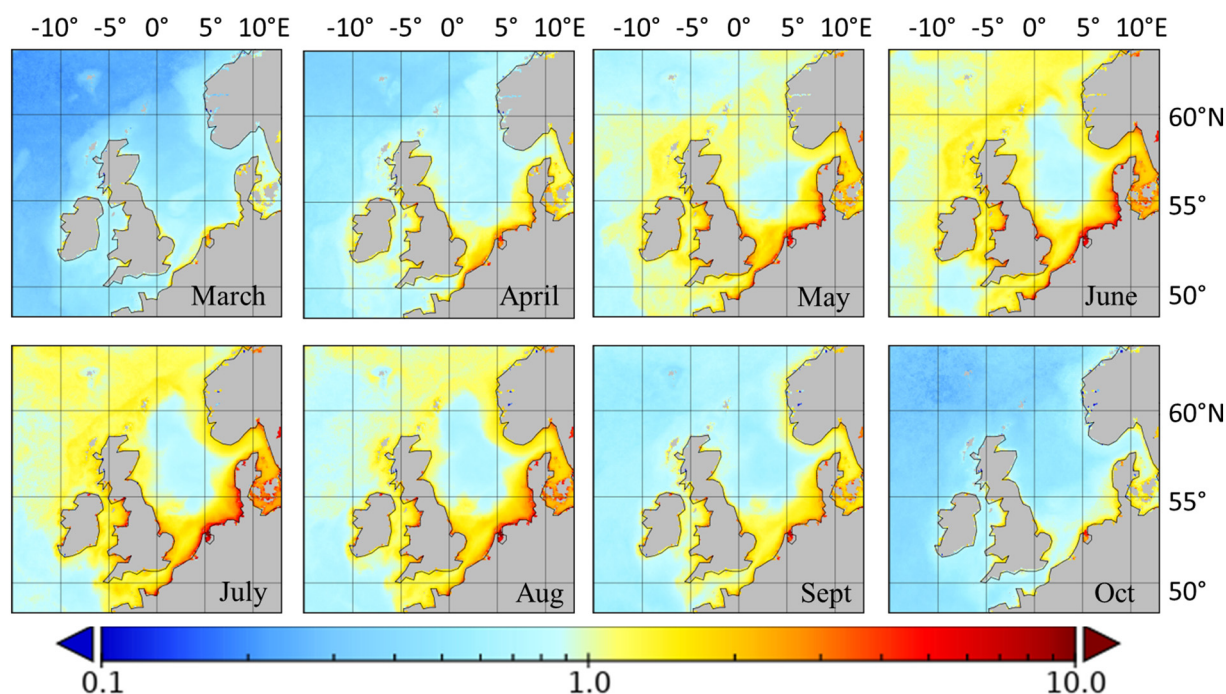


Fig. 1. Mean monthly primary production ($\text{g C m}^{-2} \text{d}^{-1}$) from March to October using CMEMS Ocean Colour data from 1997 to 2018 for the north-east Atlantic and north-west European Shelf. Case 2 water type areas are masked.

each region, counting diagonal neighbours as half to obtain a second proximity measure $p_{2i} = n_i/6$. The overall proximity to region i is then $p_{1i} + p_{2i}$. Any pixel with proximity to another region greater than to its own is reallocated to that region, keeping track of previously changed pixels to avoid infinite loops. The clustering was performed with values of N from six to 12, and $N = 11$ was chosen as the best representation of the principal hydrographic areas in the NE Atlantic (Fig. 2).

To define the upper limit of PP over the region, climatological P90 over the reference period 1997–2005 was determined at each pixel over the entire area to capture the maximum variability in PP as a threshold (Fig. 3). Daily PP P90 at a given pixel and date was defined such that 90 % of the satellite-derived PP values at that location within ± 7 days were below P90, while climatological PP P90 at a given pixel and day of year was defined such that 90 % of the satellite-derived PP values in the reference period at that location within ± 1 day were below P90 (Gohin, 2011). To reduce small-scale perturbations in the PP upper limit, climatological P90 was smoothed using a Savitzky-Golay filter of width 21 and order 3. To determine whether there is any environmental perturbation over the region on a daily basis, be it due to eutrophication, climate change or other anomalies, PP can be compared with climatological PP P90. This comparison can be made at a single point (e.g. an *in situ* measurement) or over a region of interest (e.g. using satellite or model data in the K-means clusters described above), in which case both PP and PP P90 are averaged over the region. If the PP P90 reference is consistently exceeded over a period of time, it is indicative of an environmental perturbation in the system. Chl *a* P90 was calculated in the same way for comparison. Having established threshold values, the time series trends in the data were examined by calculating the cumulative anomaly in PP and PP P90 and the temporal gradient in these parameters in each region over the whole time series.

2.4. Case studies

2.4.1. The Eyjafjallajökull volcano

The Eyjafjallajökull volcano started producing a large ash plume on 14th April 2010, causing significant iron deposition into the Iceland basin

and North Atlantic until 22nd May 2010 (Achterberg et al., 2013). CMEMS Chl *a* and PP were used to detect any signal from the volcanic ash deposition over the area from 59 to 62°N, 11 to 15.5°W.

2.4.2. Nutrient input to the coastal Wadden Sea - North Sea area

The area adjacent to the Wadden Sea is influenced by nutrient inputs from the Rhine and Maas rivers (van Beusekom et al., 2019), which are then transported northward along the Netherlands and German coast by a predominant cyclonic gyre, which can reverse under easterly winds (Sundermann and Pohlmann, 2011). Data were extracted from a rectangular area adjacent to the Wadden Sea, with the corners of the rectangle being at 52.92°N, 4.83°E; 53.37°N, 5.81°E; 53.74°N, 5.60°E; 53.9°N, 4.62°E (Fig. A1). Using daily model salinity, pixels were partitioned dynamically into estuarine, coastal and offshore over the whole time series (OSPAR, 2017), offshore having negligible occurrence within the rectangle. Figure A1 shows the relative frequency with which a given location is classified as estuarine (blue) or coastal (yellow), with white pixels being classed as both equally. Salinity, total nitrogen and phosphorus data were extracted from the coupled physical-biogeochemical model simulation described by Kerimoglu et al. (2020), and were used to identify years with high and low nutrient loads in coastal and estuarine areas. Following OSPAR (2017), estuarine waters were defined on a given day as having salinity <30, coastal as salinity between 30 and 34.5 and offshore as salinity >34.5. Relationships between the modelled total nitrogen and phosphorus, CMEMS Chl *a* and PP P90, were analysed separately in estuarine and coastal waters to assess whether Chl *a* and PP P90 thresholds were exceeded within the west-Frisian Wadden Sea area during years of high total nitrogen input.

3. Results

3.1. Trends in PP based on climatology, phenology, latitude, peak and annual rates

Fig. 1 shows mean monthly PP from March to October, illustrating the migration of the spring bloom from south to north and the variability in

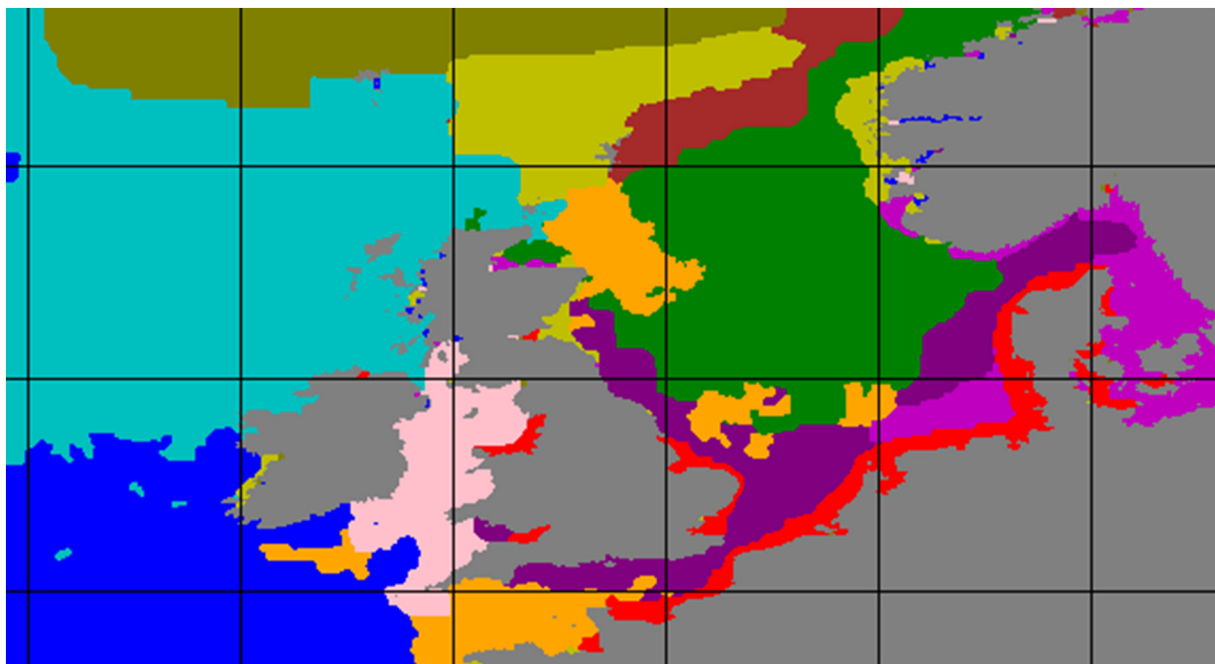


Fig. 2. Regions of similar peak, timing, location and annual primary production identified using k-means cluster analysis. Eleven regions are identified: 1.) Celtic Sea (dark blue); 2.) north-east Atlantic (light blue); 3.) northern North Sea and eastern Norwegian Sea (green); 4.) North Atlantic (olive); 5.) Faroe-Shetland Channel and Norwegian coast (yellow/green); 6.) western English Channel and parts of the North Sea (orange); 7.) central Norwegian Sea (brown); 8.) Irish Sea (pink); 9.) southern North Sea, UK coast and Skagerrak (dark purple); 10.) Kattegat, south-east North Sea and southern Norwegian coast (magenta); 11.) north-west European coast (red).

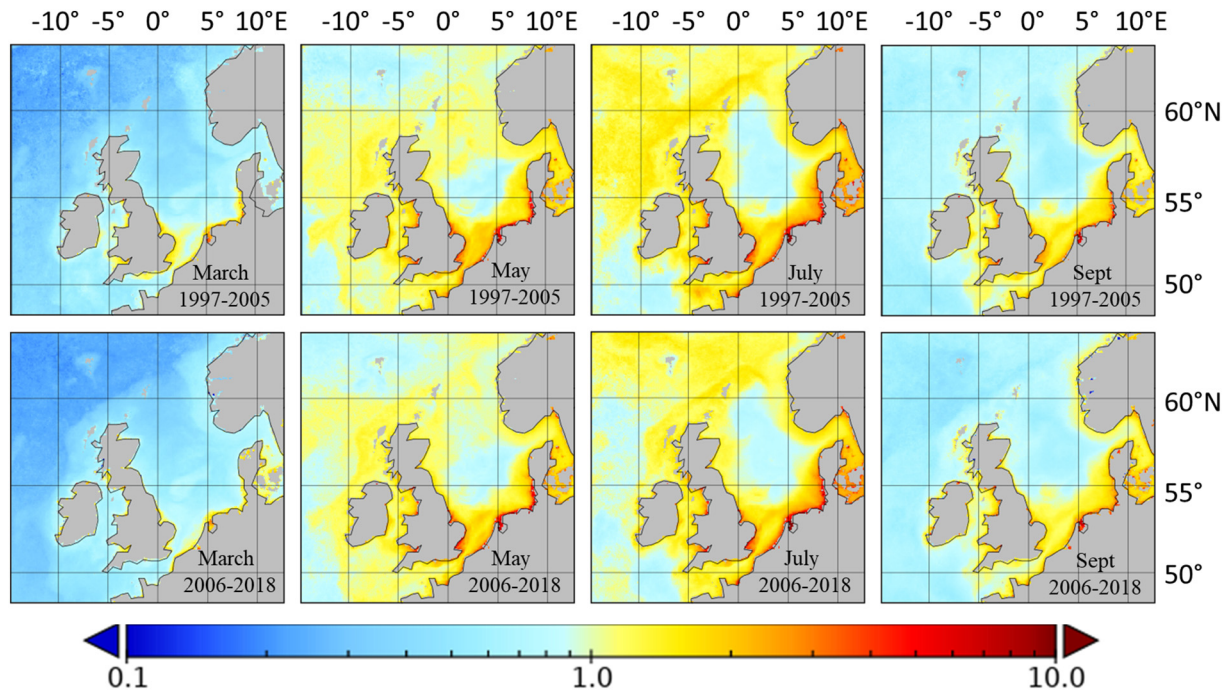


Fig. 3. Mean monthly primary production 90th percentile ($\text{g C m}^{-2} \text{d}^{-1}$) for March, May, July and September using CMEMS Ocean Colour data from 1997 to 2005 and 2006–2018 for the north-east Atlantic and North-West European Shelf. Case 2 water type areas masked.

PP over the region. In the Celtic Sea and English Channel, PP reached maximum values of $\sim 0.9 \text{ g C m}^{-2} \text{d}^{-1}$ in June and $\sim 1.0 \text{ g C m}^{-2} \text{d}^{-1}$ in July, respectively. In the central North Sea PP peaked at $\sim 0.5 \text{ g C m}^{-2} \text{d}^{-1}$ during June, and in NW European Shelf waters PP reached $\sim 1.2 \text{ g C m}^{-2} \text{d}^{-1}$ during May to July. In the NE Atlantic, PP peaked in July at $1.2 \text{ g C m}^{-2} \text{d}^{-1}$. PP was at its lowest over the entire area during March and October when 90 % of PP was between 0.2 and $1.0 \text{ g C m}^{-2} \text{d}^{-1}$.

The K-means cluster analysis of monthly PP from 1997 to 2005 based on peak PP, timing, annual PP and location, identified 11 distinctive regions (Fig. 2).

We label these based on their approximate locations as: 1.) Celtic Sea; 2.) north-east Atlantic; 3.) northern North Sea and eastern Norwegian Sea; 4.) North Atlantic; 5.) Faroe-Shetland Channel and Norwegian coast; 6.) western English Channel and frontal areas of the North Sea; 7.) central Norwegian Sea; 8.) Irish Sea; 9.) southern North Sea, UK coast and Skagerrak; 10.) Kattegat, south-east North Sea and southern Norwegian coast; 11.) North-west European coast.

3.2. Monthly and annual 90th percentile of primary production

Climatological mean monthly PP P90 from CMEMS ocean colour data over the period 1997 to 2005 were used to determine threshold values for the 11 regions identified in Fig. 2. Mean monthly PP P90 for March, May, July and September from 1997 to 2005 illustrate the spatial and temporal variation in bloom initiation, peak and decline across the region during these periods (Fig. 3). By comparison, mean monthly PP P90 from 2006 to 2018 for the same months indicate a general decrease in PP P90 compared to the period from 1997 to 2005 (Fig. 3). The associated pattern in smoothed PP P90 climatology for each of the 11 regions identified by k-means cluster analysis is shown in Fig. 4. The shape and magnitude of the climatology differed between regions, the closest in shape and magnitude being the N Atlantic and northern North Sea. The lowest mean peak climatology was in the Celtic Sea, reaching $1.0 \pm 0.25 \text{ g C m}^{-2} \text{d}^{-1}$ in June and the highest mean was in the NW European coastal waters, reaching $3.0 \pm 1.5 \text{ g C m}^{-2} \text{d}^{-1}$ during July (Table 1). The timing of the PP P90 peak varied between regions and was earlier in May in the central North Sea; in June in the northern and southern North Sea and Celtic Sea; in July in the NE

Atlantic, Kattegat and western English Channel, and as late as August in the English Channel and Faroe-Shetland region (Fig. 4).

The 1997–2005 climatological reference PP P90 (shown as solid lines and shaded areas in Fig. 4) was compared with a PP P90 climatology computed from 2006 to 2018 (shown as dashed and dotted lines in Fig. 4). The principal changes are an increase in early July and a decrease in August–September in the N Atlantic; a strong decrease from July to September in the NE Atlantic; an increase in June and a decrease in July–September in the Faroe-Shetland Channel; increases in April and August–September in the Celtic Sea and an increase in February–March and a decrease in August in the western English Channel.

3.3. Trends in primary production in relation to the 90th percentile reference

Fig. 5 shows a timeline of daily mean PP in each region (coloured lines, smoothed in the same way as climatological PP P90 for clarity) with the daily mean 1997–2005 PP P90 climatological threshold from Fig. 4 superimposed in grey. When the mean PP P90 is exceeded by PP in a region for an extended period, it indicates a potential disturbance, either natural or anthropogenic, in the ecosystem. Generally, PP stayed mostly below the PP P90 threshold except in the N Atlantic and northern N Sea. In these regions, PP consistently exceeded PP P90 especially between 2006 and 2014 in the N Atlantic and from 2011 to 2015 in the northern N Sea (Fig. 5). There were some specific years in other regions where PP was often higher than PP P90, such as 2012 in the Celtic and Irish Seas and 2006 in the Kattegat and NW European coastal regions, but these were not as prominent as the N Atlantic and northern N Sea anomalies.

Fig. 6 shows interannual variations in annual mean PP from 1997 to 2018, calculated in two ways. In the first lower estimate, daily data missing due to lack of winter Chl *a* measurements were counted as zero PP. In the second upper estimate, PP was interpolated across the winter gap. The space between is shaded. Horizontal coloured lines show the 90th percentile over all years of the two estimates, and the mean of these can be used as a threshold of annual PP. The black line is the $300 \text{ g C m}^{-2} \text{y}^{-1}$ threshold set by Boalch (1987).

Annual mean PP was $<330 \text{ g C m}^{-2} \text{y}^{-1}$ and annual mean PP P90 was $<350 \text{ g C m}^{-2} \text{y}^{-1}$, except in the Kattegat and NW European coast where

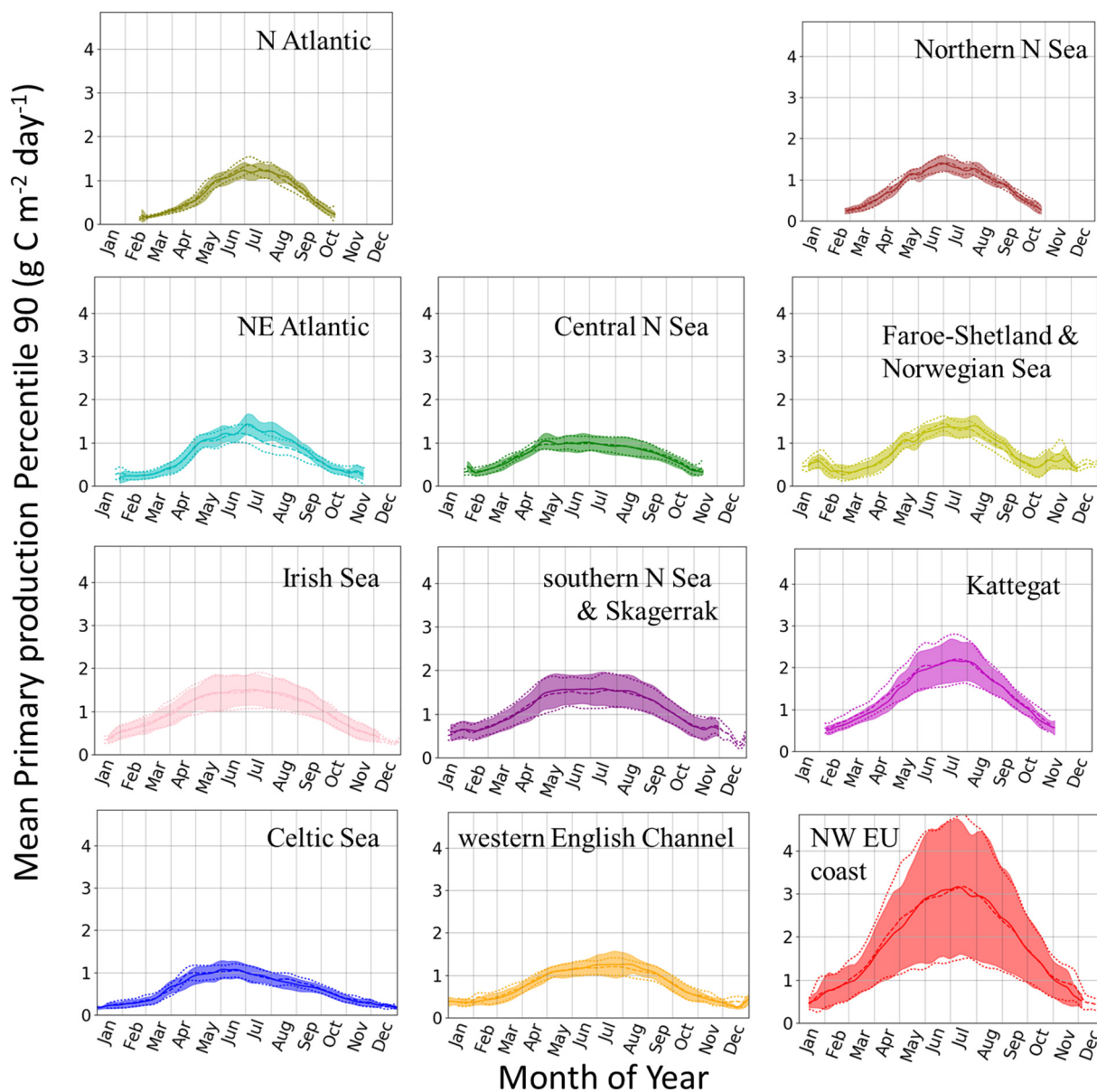


Fig. 4. Climatological mean of 90th percentile of primary production ($\text{g C m}^{-2} \text{d}^{-1}$) from 1997 to 2005 (solid line and shaded areas) and 2006 to 2018 (dashed and dotted lines) for each of the eleven regions identified in Fig. 3, with case 2 mask applied. Colours correspond to the regions given in Fig. 2.

Table 1

Thresholds in peak mean monthly and annual primary production in the eleven regions identified in Fig. 2. The first column is the mean over all years of the peak mean monthly primary production during the year, and the second (the determined threshold for monthly primary production) is the 90th percentile of this over all years. The third column is the mean annual PP over all years and the fourth (the determined threshold for annual primary production) is the 90th percentile of annual PP over all years. Each value in the third and fourth columns is the average of the upper and lower limits shown in Fig. 6.

Area	Peak mean monthly PP ($\text{mg C m}^{-2} \text{d}^{-1}$)	Peak monthly PP P90 ($\text{mg C m}^{-2} \text{d}^{-1}$)	Mean annual PP ($\text{g C m}^{-2} \text{y}^{-1}$)	Mean annual PP P90 ($\text{g C m}^{-2} \text{y}^{-1}$)
Celtic Sea	998	1246	201	228
Irish Sea	1426	1558	282	316
NW European Shelf	2756	3117	522	597
English Channel	1188	1276	254	274
southern N sea	1481	1593	317	341
Kattegat	2115	2368	384	439
central N Sea	981	1071	206	226
north-east Atlantic	1143	1397	191	221
North Atlantic	1177	1371	177	221
northern North Sea	1239	1468	181	221
Faroe-Shetland	1272	1443	240	277

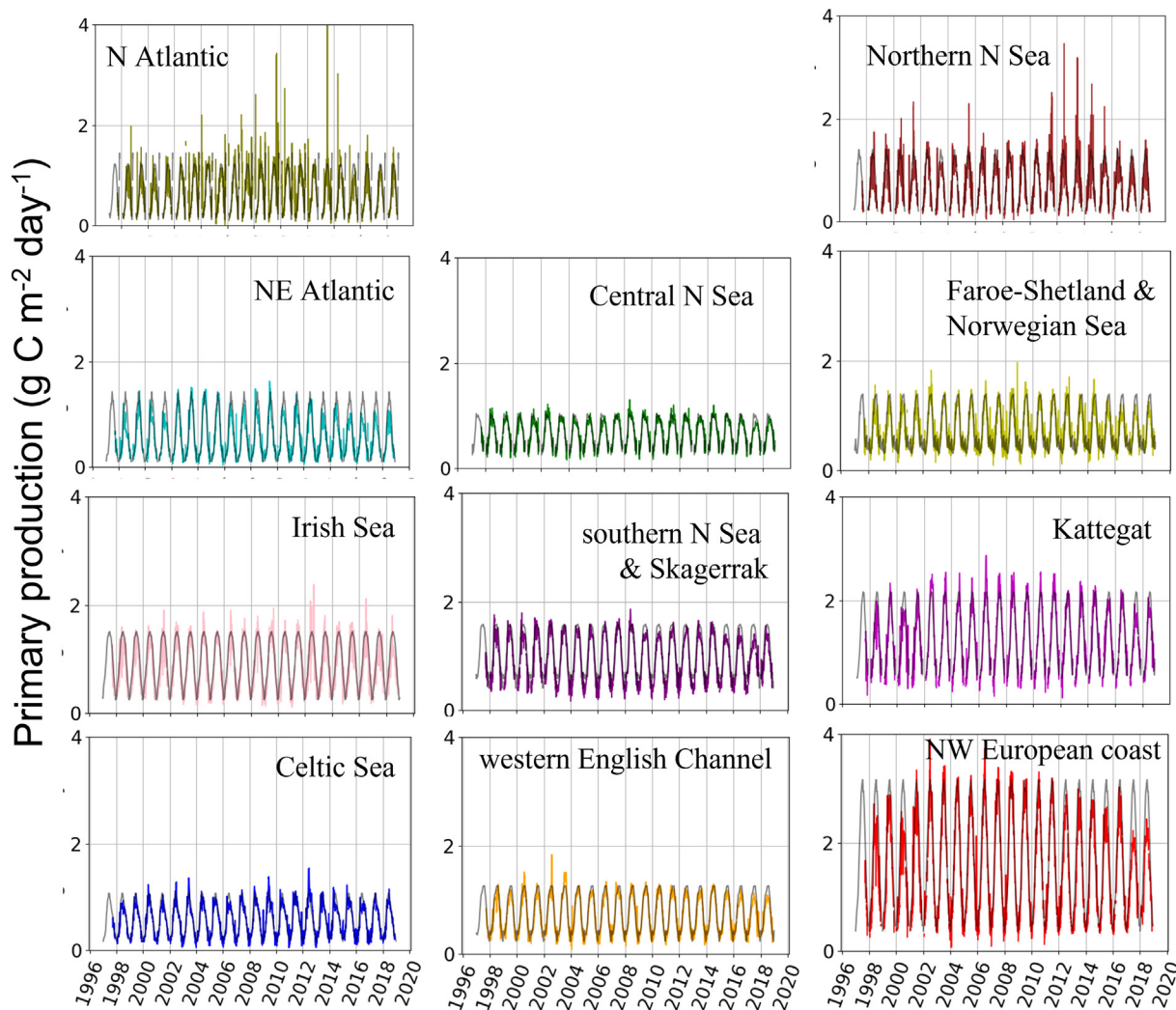


Fig. 5. Primary production ($\text{g C m}^{-2} \text{d}^{-1}$) time series for each of the eleven regions identified in Fig. 2, with case 2 mask applied. Colours correspond to the regions given in Fig. 2. Solid grey line is the climatological mean PP P90 for the reference period (1997–2005) given in Fig. 4.

annual mean PP were 384 and $522 \text{ g C m}^{-2} \text{y}^{-1}$, respectively (Fig. 6, Table 1). Areas with annual mean PP $< 300 \text{ g C m}^{-2} \text{y}^{-1}$ (the historic threshold) include the N and NE Atlantic, northern North Sea and Celtic Sea ($\sim 200 \text{ g C m}^{-2} \text{y}^{-1}$), the Faroe-Shetland Channel ($240 \text{ g C m}^{-2} \text{y}^{-1}$), English Channel ($250 \text{ g C m}^{-2} \text{y}^{-1}$) and Irish Sea ($280 \text{ g C m}^{-2} \text{y}^{-1}$).

3.4. Detecting disturbances in the marine environment using thresholds in primary production 90th percentile

To assess whether PP P90 can be used to detect disturbances in the marine environment, two case studies were examined; one in the open ocean caused by a natural volcanic eruption and the other in the coastal zone due to anthropogenic input of nitrogen. Firstly, the area between Iceland and Scotland to the south-east of the Iceland basin was analysed to detect effects of volcanic ash from the eruption of the volcano, Eyjafjallajökull, during April and May 2010 (Fig. 7). This is predominantly (93 % of pixels) within the NE Atlantic region (Fig. 2). The ocean colour satellite composite images over the period of the volcanic eruption illustrate that there were relatively high, but heterogenous, Chl *a* and PP values (Fig. 7a, b). Time series of PP and Chl *a* over this area from 1st March to 15th October 2010 are given in Fig. 7c, d and in more detail from 20th April to 8th June 2010 in Fig. 7e, f. The time series data clearly show that from 28th April 2010 both the daily mean Chl *a* and PP increased sharply until 6th May (red line in Fig. 7c, d, e, f) but that PP and Chl *a* do not exceed the

climatological (1997–2005) PP P90 and Chl *a* P90 thresholds in the NE Atlantic region (blue line in Fig. 7c, e). PP is closer to the threshold than Chl *a* as can be seen during the periods from 28th April to 6th May and 18th to 27th May. By contrast, the climatological (1997–2005) Chl *a* P90 threshold in the NE Atlantic region was only exceeded on 4th May 2010 (blue line in Fig. 7d, f). The distance between the upper limit of the Chl *a* standard deviation and the Chl *a* P90 was always greater than that between the upper limit of the PP standard deviation and the PP P90, suggesting that PP P90 may be a more sensitive threshold than Chl *a* P90 in the open ocean.

The second case study was along the North Sea coast adjacent to the Wadden Sea, which was dynamically segregated on a daily basis into coastal and estuarine waters using model surface salinity values (OSPAR, 2017) the location of which is given in Fig. A1. Fig. 8 shows daily mean time series data (red line) and mean daily climatology and standard deviation from 2006 to 2014 (dashed black line and grey shaded area) for PP, Chl *a*, TN and TP in estuarine and coastal waters from 1st February to 1st November 2007. In addition, 1997–2005 PP P90 (Fig. 8a, e) and Chl *a* P90 (Fig. 8b, f) averaged over the specific box area of study (52.92°N , 4.83°E ; 53.37°N , 5.81°E ; 53.74°N , 5.60°E ; 53.9°N , 4.62°E) in estuarine and coastal waters are shown as a blue line and the OSPAR (2017) thresholds for Chl *a* (Fig. 8f), winter TP (Fig. 8c, g) and winter TN (Fig. 8d, h) are given as the green line.

In both coastal and estuarine cases, TP and TN were above the winter threshold during February to early May, reaching $1.5 \mu\text{mol L}^{-1}$ TP

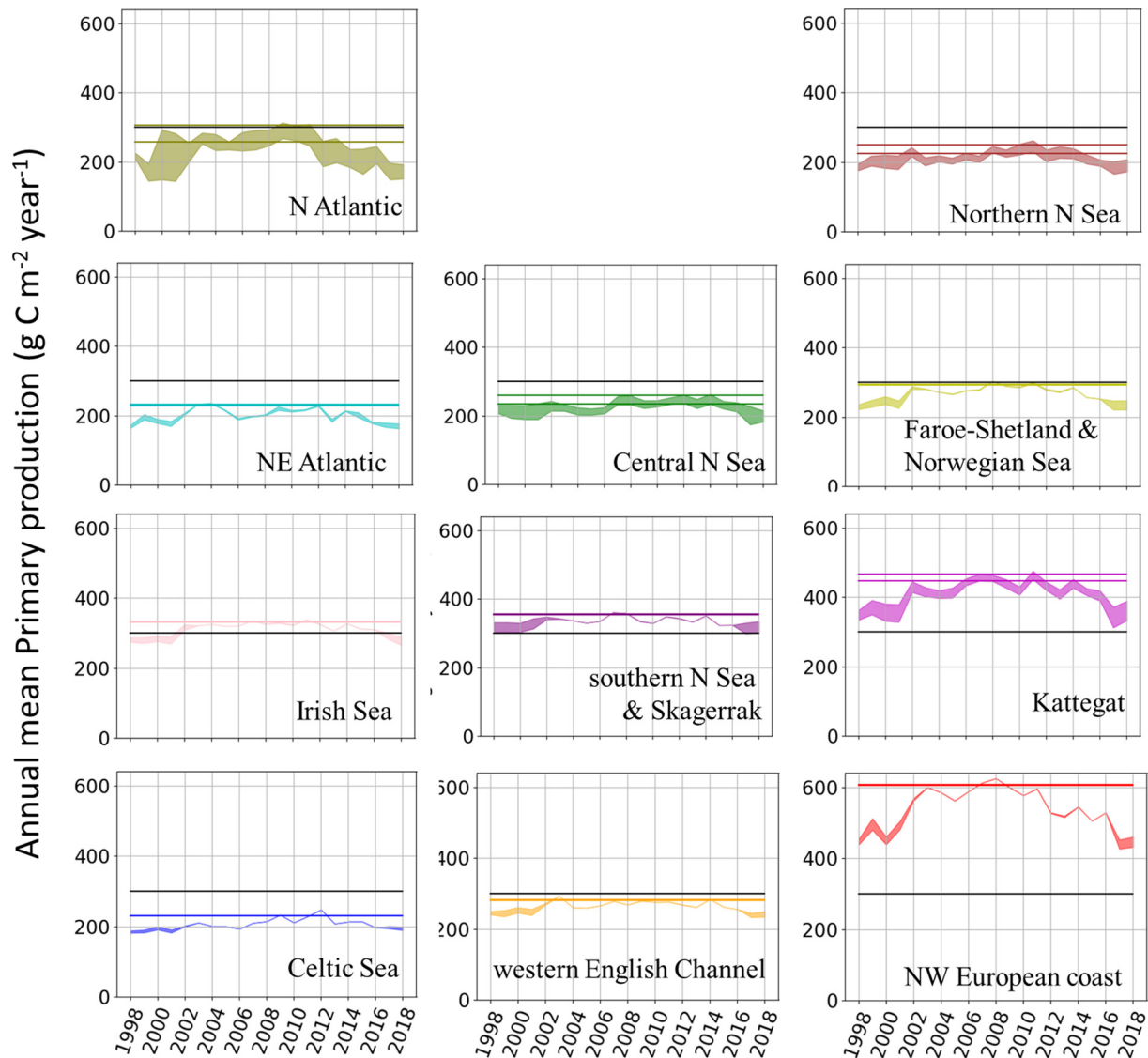


Fig. 6. Time series of annual primary production ($\text{g C m}^{-2} \text{y}^{-1}$) in the eleven regions identified in Fig. 2, with case 2 mask applied. The upper and lower limits of the time series show two ways of representing missing data: the upper limit interpolates PP between November to February, while the lower limit assumes a PP of zero from November to February. Colours correspond to the regions given in Fig. 2. The coloured lines represent the new determined thresholds (90th percentile of annual primary production from 1997 to 2005) for each region based on these ways of integrating the data. The solid black line is the threshold derived by Boalch (1987) and Boalch et al. (1978).

(Fig. 8c, g) and $> 60 \mu\text{mol L}^{-1}$ TN (Fig. 8d, h), respectively. The response to these high nutrient loads by phytoplankton could be detected as high Chl *a* and PP at the end of March to mid-May (Fig. 8a, b, e, f). During this period in the estuarine area, PP and Chl *a* rarely went above the PP P90 and Chl *a* P90 thresholds for the box area (Fig. 8a) and Chl *a* P90 thresholds for the box area (Fig. 8a) and Chl *a* P90 threshold of 18 mg m^{-3} . By contrast, in the coastal area both PP and Chl *a* exceeded these thresholds periodically from the end of April to the beginning of May (Fig. 8e, f), indicative of the high TN and TP during the previous months. PP and Chl *a* also exceeded these thresholds at the beginning of June, though this was likely due to the influence of other parameters such as PAR and/or temperature. Similar to the volcanic eruption case study, the maximum PP values in the standard deviation were closer to the PP P90 threshold compared to Chl *a* and the Chl *a* P90 threshold, again suggesting that PP may be a more sensitive indicator of anthropogenic disturbances.

4. Discussion

This study addresses two questions on using satellite ocean colour data to identify disturbances in the marine environment:

1. Are there differences in climatological and phenological characteristics between Chl *a* and PP, which would make one of the parameters more sensitive to detecting disturbances?
2. Can PP be used as an indicator of disturbances in the marine environment and if so, how do long term trends differ between studies? These questions are explored in more detail, below.

4.1. Similarities in climatological and phenological regional traits

Analysis of phenological and climatological characteristics offers potential insight into the variability in phytoplankton seasonal cycles in relation to environmental forcing, disturbance and anomalies (Racault et al., 2012; Sarmiento et al., 2004). For example, using merged GlobColour satellite data (with the GSM Chl *a* algorithm), Friedland et al. (2018) indicated that the bloom start date, magnitude and duration in the NE Atlantic and North Sea is highly variable, with the start date ranging from day 60 to 180 and duration lasting from 40 to 70 days. Bloom initiation has been related to the winter mean net heat flux and wind speed (Cole et al., 2015; Henson et al., 2006), the timing of which is linked to the North Atlantic Oscillation (Henson et al., 2009; Tilstone et al., 2015; Zhai et al., 2013).

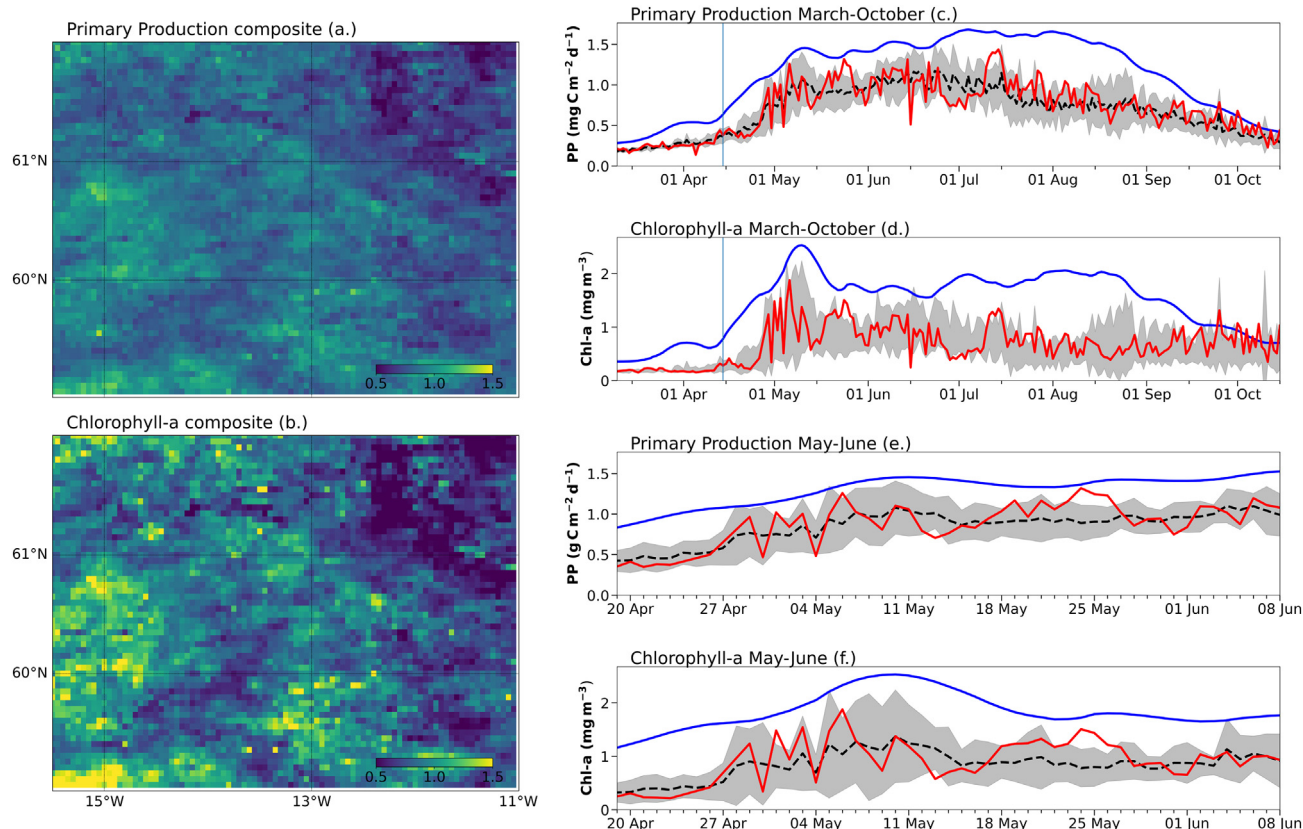


Fig. 7. Composite images of (a.) primary production ($\text{g C m}^{-2} \text{d}^{-1}$) and (b.) Chlorophyll-*a* (mg m^{-3}) from April to May 2010 during the period of the Eyjafjallajökull volcanic eruption and time series of (c.) primary production ($\text{g C m}^{-2} \text{d}^{-1}$) and (d.) Chlorophyll-*a* (mg m^{-3}) from March to October 2010, (e.) primary production ($\text{g C m}^{-2} \text{d}^{-1}$) and (f.) Chlorophyll-*a* (mg m^{-3}) from 20th April to 8th June 2010. Black dashed line is the mean daily climatology from 1997 to 2016; grey shaded area is the standard deviation of the mean climatology from 1997 to 2016; red line is the mean daily value for 2010. The solid blue lines are the climatological threshold of PP P90 and Chl *a* P90 for the NE Atlantic, respectively.

Distinctive phenological properties derived from remote sensing ocean colour data have been used to assess the impacts of climate change on phytoplankton bloom development in coastal, shelf and oceanic environments (Krug et al., 2018). Recent studies on phenology in the North Sea, based on OC-CCI time series data from 2000 to 2020, have shown that the spring bloom now starts earlier, and the duration is longer (Silva et al., 2021). This has been related to shallower mixed layer depths limiting the resuspension of suspended material to the surface which results in more stratified, clearer waters, which in turn form higher biomass blooms. Similarly, in the greater North Sea, the spring bloom has been observed to be occurring earlier with a one month difference between 1998 and 2020 and longer duration, which is partially explained by rising seawater temperatures (Alvera-Azcarate et al., 2021). In addition, summer blooms have been observed to start and end later, and to be longer in duration with higher Chl *a* concentrations (Silva et al., 2021). Using 21 years of merged ocean colour data, we identified that the highest PP in the NE Atlantic and North Sea occurs between May and July (Fig. 4). By comparison, (Silva et al., 2021) illustrated a contrasting climatology in the central North Sea and German-Denmark coastal sub-regions, with a shallow Chl *a* peak in April and the lowest biomass in July. Using MODIS-Aqua data, Naustvoll et al. (2020) characterised a double peak in Chl *a* for the Iceland Basin, with a maximum in April followed by a secondary peak in September. By contrast, Taboada and Anadon (2014) observed a single spring-summer peak from merged SeaWiFS-MODIS-Aqua data (with the GSM Chl *a* algorithm) for the NE Atlantic similar to the climatology that we observe in PP for this region (Fig. 4), but with a shorter duration. A similar climatological shape has also been characterised using *in situ* data for the Faroe-Shetland shelf (Eliassen et al., 2017) in 1999–2001, 2004, 2008 and 2014. The trends in climatology presented in this paper possibly reflect

that spring and summer blooms have become longer, but it may also be that when monthly data are used, the spring-summer bloom periods merge. In addition, the fact that the Chl *a* climatology does not always reflect peak and duration in PP, also highlights potential differences between the uses of Chl *a* and PP to characterise the phenology and climatology, since PP is also dependent on the available light in the water column and the physiological state of phytoplankton. Based on similarities in climatological PP, phenology, latitude and longitude, we characterised the study area into 11 distinct regions (Fig. 2). These regions broadly map onto the salient hydrographic conditions, for example: region 2 (NE Atlantic) corresponds to the area occupied by east North Atlantic water; region 5 (Faroe-Shetland Channel) reflects the inflow of North Atlantic water between Faroe-Shetland and northern Scotland; region 9 corresponds to the inflow of water from the English Channel and southern bight of the North Sea; region 10 corresponds to the outflow of Baltic seawater through the Kattegat and Skagerrak and region 11 corresponds with NW coastal regions (Reid et al., 1988).

4.2. Derivation of threshold indicators from satellite ocean colour primary production 90th percentile data

Many countries established national programs in the 1980's and 1990's using specific *in situ* data to monitor the environment. Chl *a* P90 was established as a key metric for assessing water quality and specifically eutrophication (OSPAR, 2003). Providing sufficient *in situ* data, especially during funding gaps and national lockdowns resulting from the recent pandemic, can be a serious limitation for monitoring programs. The increasing availability of remote sensing ocean colour has broadened the possibilities of utilising satellite Chl *a* as a synoptic tool to provide high spatial and temporal resolution data over long time-series. These data have become more and

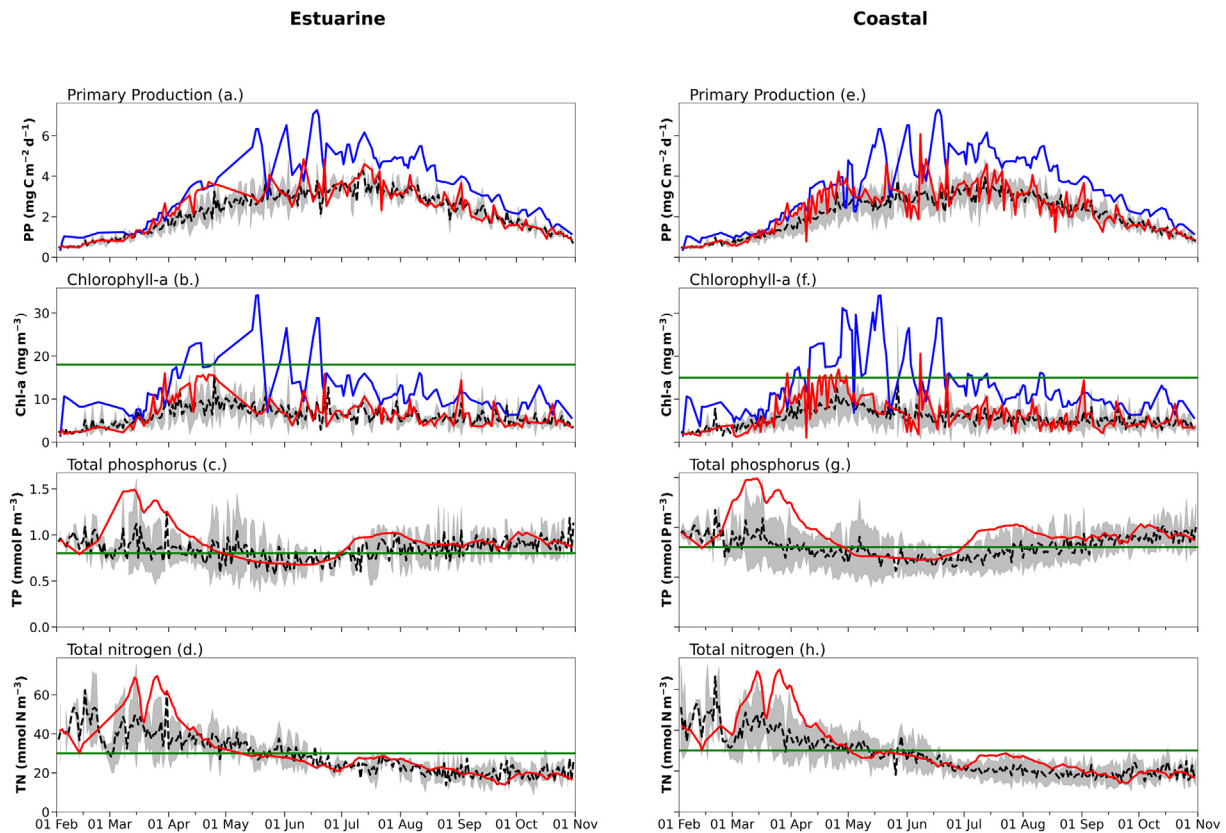


Fig. 8. Time series of (a, e) primary production ($\text{g C m}^{-2} \text{d}^{-1}$), (b, f) Chlorophyll-*a* (mg m^{-3}), (c, g) total phosphorus ($\mu\text{mol L}^{-1}$) and (d, h) total nitrogen ($\mu\text{mol L}^{-1}$) from February to November 2007 for estuarine and coastal regions derived from an area in the NW European coast adjacent to the Wadden Sea (shown in the salinity field figure). For each time series plot, the dashed black line is the mean daily climatology from 2004 to 2016; grey shaded area is the standard deviation of the mean climatology from 2004 to 2016; red line is the mean daily value for 2007. In (a, b, e, f) the solid blue line is the PP P90 and Chl *a* P90 threshold for the study area. In (b, f), the horizontal green line is the Chl *a* threshold defined by OSPAR (2017) for Dutch estuarine and coastal waters. In (c, g) the winter DIN and in (d, h) the winter DIP limit for the Dutch coast as defined by OSPAR (2017) are also given as the green lines.

more accurate over recent decades (Tilstone et al., 2017; Tilstone et al., 2021) and are being evaluated for operational use by OSPAR for the next GES Assessment due in 2022–23. Trends in water quality have been successfully monitored using a combination of *in situ* and satellite data (Gohin et al., 2019; Harvey et al., 2015). Directives and policies made internationally and nationally have restricted and reduced pollutants entering the marine environment. The effectiveness of some of these directives has led to a reduction in N, P and/or Chl *a* in some areas (Gohin et al., 2019) to below Chl *a* P90 thresholds, but not in others (Arabi et al., 2020).

Prior to using PP P90 for monitoring the environment, the natural limit in daily and annual rates needs to be quantified. Previous studies have estimated annual production for the North Atlantic to be $238 \pm 22 \text{ g C m}^{-2} \text{ yr}^{-1}$ (Zhai et al., 2012). Within the North Atlantic, over the Icelandic Reykjanes Ridge and in the Iceland Basin it is estimated to be 221 ± 40 and $204 \pm 33 \text{ g C m}^{-2} \text{ yr}^{-1}$, respectively (Tilstone et al., 2014; Tilstone et al., 2015). In this study we found that mean annual production values for the open ocean were similar and varied from $177 \text{ g C m}^{-2} \text{ yr}^{-1}$ in the north Atlantic to $191 \text{ g C m}^{-2} \text{ yr}^{-1}$ in the north-east Atlantic (Fig. 7; Table 1). In coastal regions, a global analysis by Cloern et al. (2014) reported a mean value from 131 ecosystems of $252 \text{ g C m}^{-2} \text{ yr}^{-1}$. The range however was large, with values as low as $105 \text{ g C m}^{-2} \text{ yr}^{-1}$ in the Scheldt Estuary and $1890 \text{ g C m}^{-2} \text{ yr}^{-1}$ in the Tamagawa Estuary. Boynton et al. (2018) reported average annual rates of $190 \text{ g C m}^{-2} \text{ yr}^{-1}$ from 45 estuaries worldwide. At a coastal station in the western English Channel, annual production is reported to be $115 \text{ g C m}^{-2} \text{ yr}^{-1}$ (Barnes et al., 2015). Based on *in situ* ^{14}C PP data, the mean annual production at Bermuda Atlantic Time Series (BATS) from 1989 to 1997 was $154 \text{ g C m}^{-2} \text{ yr}^{-1}$ (Steinberg et al., 2001). Using 21 years (1998 to 2018) of satellite-based annual climatological PP values, we were able to re-define

thresholds for each region, by calculating the 90th percentile of annual mean PP. These varied from $221 \text{ g C m}^{-2} \text{ yr}^{-1}$ in the north-east Atlantic, N Atlantic and northern N Sea to $597 \text{ g C m}^{-2} \text{ yr}^{-1}$ along the NW European coast (Fig. 5, Table 1). For eight out of the eleven regions identified by k-means cluster analysis, the mean annual PP was less than the previously defined $300 \text{ g C m}^{-2} \text{ yr}^{-1}$ threshold (Boalch, 1987; Boalch et al., 1978). Only the NW European coast, Kattegat and southern North Sea had mean annual PP that exceeded this threshold. The NW European coast had the largest annual production with mean PP (PP P90) values of 522 (597) $\text{g C m}^{-2} \text{ yr}^{-1}$, followed by the Kattegat with 384 (439) $\text{g C m}^{-2} \text{ yr}^{-1}$ and then the southern North Sea with 317 (341) $\text{g C m}^{-2} \text{ yr}^{-1}$ (Fig. 6; Table 1). The regionally defined thresholds offer a novel way of assessing perturbations in the environment due to an array of factors including anthropogenic disturbances such as eutrophication, in coastal waters, and climate change. These trends in PP P90 have not been reported previously and represent an upper limit of PP in the ecosystem, whilst eliminating outliers.

In the N Atlantic and at higher northern latitudes, nutrients are often replete and enhanced stratification may actually augment PP by subjecting phytoplankton to a higher light regime (Bopp et al., 2001; Doney, 2006; Stock et al., 2014). From our data in the NE Atlantic, the time series suggests an increase in PP from 1997 to 2004, and a decrease from 2012 to 2018 (Fig. 5). Similarly, McQuatters-Gollop et al. (2011) observed an increase in Chl *a* from 1995 to 2010 in the north Atlantic using the colour index derived from continuous plankton recorder data. Further south west at the Bermuda Atlantic Time Series (BATS) in the Sargasso Sea, (Lomas et al., 2010) showed from *in situ* ^{14}C measurements that there was a steady increase in PP from 1989 to 2007 by approximately 2 % over this period. In the greater North Sea, Alvera-Azcarate et al. (2021) also

observed an increase in satellite Chl *a* from 1998 to 2008 and a decrease from 2014 to 2019. In the North Sea, we observed contrasting patterns in PP P90 and annual rates. PP in the central and southern North Sea remained constant, whereas in the northern N Sea, it was far more variable with peak values in daily and annual rates from 2011 to 2014 (Fig. 5). In coastal areas of the North Sea, trends in Chl *a* concentration can be influenced by rising sea surface temperatures and the reduction in nitrogen and phosphorus loads following the implementation of the Water Framework Directive (WFD). In the southern and central North Sea, Desmit et al. (2020) observed a decline in annual Chl *a* from 1988 to 2016 and a shift to earlier spring blooms, though there was no clear correlation for this with temperature and winter nutrients. By contrast, Capuzzo et al. (2018) showed that there was a steady decline in annual PP in the seasonally stratified N Sea from 1998 to 2012, though there was a prominent increase in PP in 2010. The differences between Capuzzo et al. (2018) and the pattern shown in our data, is likely to be due to the PP model used. The Capuzzo et al. (2018) model is empirical and based on the linear regression between Chl *a* and the PAR attenuation coefficient K_d . The model we deployed is semi-analytical and resolves the spectral light field in relation to Chl *a* and the photosynthetic quantum yield (Smyth et al., 2005), as well as omitting optical case 2 areas where both satellite estimates of Chl *a* and PP can be less accurate. In the English Channel, there was a slight but gradual decline in PP from 2002 to 2014 (Fig. 5). A similar decline in Chl *a* has also been seen in French coastal areas of the English Channel, which is related to a decrease in riverine phosphorus as a result of successful implementation of nutrient reduction measures under the WFD (Gohin et al., 2019).

Over the satellite ocean colour time series, there could potentially be a bias between satellite sensors. During the first half of the reference period from 1997 to early 2002, the only ocean colour satellite used was SeaWiFS and from 2002 on, the satellite data came from combinations of four different sensors (SeaWiFS, MODIS-Aqua, MERIS, VIIRS). The method of merging the data uses SeaWiFS remote sensing reflectance as the reference where possible and normalises the data from the other sensors to this (Melin et al., 2017), so theoretically there should be no bias in the resulting Chl *a* concentrations. Any bias between these periods would arise from differences in cloud free observations from several different satellite sensors as opposed to one during the SeaWiFS-only period (Alvera-Azcarate et al., 2021). There are different merged ocean colour products available. No independent validation to compare these products has been undertaken thus far. It is recommended that this is done in the future so that the most accurate product is utilised to assess longer term trends and potential disturbances in the marine environment.

4.3. Is primary production an indicator of disturbances in the marine environment?

The natural cycle of water column mixing and nutrient enrichment in the photic zone followed by stratification and high light availability promotes an increase in Chl *a* at the onset of the spring bloom (Sverdrup, 1957). This is then followed by a crash in Chl *a* as nutrients become limiting. This natural cycle is easily discernible from space using satellite ocean colour data (Blondeau-Patissier et al., 2014). PP in most temperate estuaries and coastal marine ecosystems is nitrogen limited (Dugdale and Goering, 1967; Howarth et al., 2021; Ryther and Dunstan, 1971). The enhanced input of nitrogen from urban and agricultural sources in some coastal regions can cause accelerated phytoplankton growth above the natural limits of the spring bloom, which in turn leads to a degradation in water quality (Tett et al., 2007). Experimental studies have shown a clear relationship between nutrient concentrations and primary productivity (Edwards et al., 2005; Loureiro et al., 2005; Ornlöfsdóttir et al., 2004). Using field data to assess this can often be problematic due to the lag time between nutrient input and phytoplankton growth (Xie et al., 2015). Variability in global PP as a result of climate change has been detected using ocean colour (Behrenfeld et al., 2006). Field fertilization experiments in the Southern Ocean, which is limited by the availability of dissolved iron, clearly demonstrated an increase in ocean colour Chl *a* visible from space

(Boyd et al., 2007; Zhang et al., 2021). The effects of large Ocean tsunamis are observable from satellite data with a concomitant increase in the ocean colour Chl *a* soon after (Sarangi, 2011; Sava et al., 2014). The recent unprecedented and devastating forest fires in Australia from September 2019 to March 2020 similarly caused a tractable signature in Chl *a* (Wang et al., 2022) and productivity (Tang et al., 2021).

Though Chl *a* P90 has been used as a standard metric to assess the effects of environmental pollution in the marine environment, PP P90 has not been used. Theoretically, changes in PP are a more robust metric than Chl *a* since the daily variability in Chl *a* can be far higher than PP (Becker et al., 2021). To our knowledge PP P90 has not been used so far as a metric to monitor environmental change or disturbance in marine phytoplankton. To test this, we used two case studies to address the questions: Can we detect environmental perturbations from the PP P90 signature? And how does this compare with Chl *a* P90?

In the first case study we assessed the effects of dust from the Icelandic volcano Eyjafjallajökull eruption on 14th April 2010. We found a clear signature in the daily Chl *a* and PP during two periods at the beginning and end of May 2010 (Fig. 7). The PP was close to or above the PP P90 threshold for the NE Atlantic on both occasions. Chl *a* and Chl *a* P90 exhibited a similar pattern, but the maximum PP was consistently closer to PP P90 compared to Chl *a*, suggesting that PP P90 may be more sensitive to this natural disturbance in the ecosystem. The decrease in both Chl *a* and PP P90 between these two periods may have been due to nutrient limitation.

The second case study was along the North Sea – Wadden Sea coast. The region receives major nutrient discharge from a number of European rivers including the IJsselmeer, Ems, Weser, Elbe, Rhine and Maas (van Beusekom et al., 2019). Residual currents along the Wadden Sea follow the predominantly cyclonic circulation of the North Sea (Sundermann and Pohlmann, 2011), which carries nutrients from the Rhine and Maas north-eastward and partially blocks nutrients from flowing westward from the other rivers that discharge directly into the Wadden Sea (Grosse et al., 2017). Eutrophication in the region was reported from the 1950's (de Jonge et al., 2002) due to artificial fertiliser from agriculture and urban wastewater (Battye et al., 2017), and reached a peak in the 1980's (Cadee and Hegeman, 2002). This caused an increase in phytoplankton and green macroalgae blooms (Smetacek and Zingone, 2013), which resulted in the loss of sea grass due to the reduction in the light field caused by these blooms. Due to the implementation of stringent measures to reduce eutrophication, total nitrogen and phosphorus levels have declined in the region as has phytoplankton Chl *a*, but N/P ratios have increased (van Beusekom et al., 2019), which may have changed the phytoplankton community composition. Based on the last OSPAR report, eutrophication is a continuing problem along the coast from Belgium to Danish and Swedish waters (OSPAR, 2017). In estuarine and coastal areas, PP can be highly variable, so we calculated a regional specific threshold for the area studied. For both estuarine and coastal areas, the daily TN and TP (red line in Fig. 8) were higher from the end of February until mid-April 2007, compared to both the mean for the reference period (2006–2014; black dotted line in Fig. 8) and the winter OSPAR thresholds (green line in Fig. 8). There was a clear lag response in daily Chl *a* and PP concentrations to the elevated nutrients and similarly, the daily Chl *a* and PP values were above the mean from 2006 to 2014, but the Chl *a* concentration was below the Chl *a* P90 OSPAR threshold for the estuarine pixels, and there were a few instances when it went above the threshold for the coastal pixels. When we applied the regional specific PP P90 threshold (blue line in Fig. 8a, e), the pattern was similar to the regional specific Chl *a* P90 threshold and the Chl *a* P90 OSPAR threshold (blue line in Fig. 8b, f), but some PP values were closer to the PP P90 threshold and/or more frequently were above the threshold, suggesting that this approach may be more sensitive compared to using Chl *a* P90. In June 2007, for the coastal pixels both Chl *a* and PP went above the reference mean (2006–2018) and the respective thresholds, which was due to other variables other than TN and TP which were low before and during this period.

In summary, in the open-ocean case where PP is relatively stable, and the variability is generally lower, by applying a broad scale k-means PP

P90 threshold, we were able to detect effects of volcanic dust on PP. In a highly dynamic coastal region in which we defined an area specific PP P90 threshold, we could detect high TN and TP signatures in a coastal area. Both cases showed that PP P90 is slightly more sensitive than Chl *a* P90 to perturbations in the marine environment. We have clearly shown that this method can detect anomalies in the environment, both natural and anthropogenic. It should be tested operationally in conjunction with existing monitoring programmes.

4.4. Future recommendations

The method we present here represents an independent means of using satellite derived PP to detect disturbances in the environment. The method could be further improved by using:

- Higher spatial resolution satellite data (e.g. 300 m Sentinel-3 OLCI);
- Independent validation of different merged ocean colour products is recommended to assess which are the most accurate for application to analysis of long term trends in Chl *a* and PP.
- Chl *a* algorithms that are accurate at high SPM and CDOM concentrations, in conjunction with high resolution data to be able to apply the method further into the coast and estuaries;
- Satellite estimates of CDOM for use in the PP model;
- Uncertainties in the PP and PP P90 data on a per pixel basis, in association with the thresholds;
- Other satellite data (e.g. SST, SSS, SSH) and other parameters available from ocean colour (e.g. size specific Chl *a* or PP) to further refine the region definitions.
- Further case studies to evaluate performance and compare PP P90 with Chl *a* P90.

5. Conclusions

21 years of satellite ocean colour data were analysed to determine daily and annual primary production percentile 90 thresholds for similar regions, identified through k-means clustering. Daily PP P90 climatology values accurately detected disturbances arising from natural volcanic dust and anthropogenic high nitrogen inputs along the North Sea – Wadden Sea coast. The thresholds are defined both as daily maximum during phytoplankton blooms and as annual rates. Eight out of eleven regions had thresholds $<300 \text{ g C m}^{-2} \text{ y}^{-1}$, which was the historic definition for the region based on data measured in the English Channel during the 1970's and 80's. The highest monthly and annual PP P90 was in the NW European coast ($3.1 \text{ g C m}^{-2} \text{ d}^{-1}$, $597 \text{ g C m}^{-2} \text{ y}^{-1}$) and the lowest was in the N Atlantic ($1.4 \text{ g C m}^{-2} \text{ d}^{-1}$, $221 \text{ g C m}^{-2} \text{ y}^{-1}$). Using PP P90 thresholds for the north-east Atlantic the effect of dust deposition from the Eyjafjallajökull volcano could be detected, and this proved to be slightly more sensitive than Chl *a* P90. Using this approach, custom specific thresholds of PP P90 can be derived for regional and smaller areas (down to 0.05° pixel level), which proved to be effective in detecting the influence of high TN and TP loads adjacent to the Wadden Sea on PP, with slightly better sensitivity than Chl *a* P90. This method represents an accurate means of determining environmental disturbances in remotely sensed ocean colour PP data, that has not previously been explored.

Supplementary data to this article can be found online at <https://doi.org/10.1016/j.scitotenv.2022.158757>.

CRediT authorship contribution statement

'Threshold indicators of primary production in the north-east Atlantic for assessing environmental disturbances using 21 years of satellite ocean colour data.' by Tilstone, Land, Pardo, Kerimoglu, van der Zande, for publication in Science of the Total Environment.

Dr. Gavin Tilstone obtained the funding to carry out the research, conceived and directed the research and wrote the paper. Dr. Peter Land processed the satellite imagery, directed the research, produced the figures and

contributed significant input to the writing of the paper. Silvia Pardo conducted the case studies, produced the associated figures and commented on the ms. Onur Kerimoglu provided the nutrient and salinity data for the coastal case study and commented on the ms. Dimitry van der Zande produced the case 2 optical water mask for processing the satellite imagery and commented on the ms.

Data availability

Daily CMEMS Chl *a* (mg m^{-3}) data are available at: https://resources.marine.copernicus.eu/?option=com_csw&view=details&product_id=OCEANCOLOUR_ATL_CHL_L3_REP_OBSERVATIONS_009_067. The daily CMEMS SST product, that was used to run the primary production model is available at: https://resources.marine.copernicus.eu/?option=com_csw&view=details&product_id=SST_GLO_SST_L4_REP_OBSERVATIONS_010_011. Daily SeaWiFS and MODIS photosynthetically available radiation (PAR), that was also used to run the primary production model is available at: <https://oceansci.gsfc.nasa.gov/directaccess/>

Declaration of competing interest

The authors declare that they have no known competing financial interests or personal relationships that could have appeared to influence the work reported in this paper.

Acknowledgements

Ocean colour imagery was provided by the Copernicus Marine Service (CMEMS) Ocean Colour product for the NE Atlantic produced by Plymouth Marine Laboratory. We are grateful to NEODAAS for hosting the data and allowing us computing capacity to process the PP images. GHT, PEL, SP and DVdZ were funded by the European Commission DG Environment (EU DG ENV) grants: JMP EUNOSAT – 'Joint Monitoring Programme of the Eutrophication of the North Sea with Satellite Data' (Contract No.11.0661/2017/750678/SUBIENV.C2) and NEA PANACEA – 'North East Atlantic project on biodiversity and eutrophication assessment integration and creation of effective measures' (Contract No.31167499). A Healthy and Biologically Diverse Seas Evidence Group project called 'Development of a UK waters specific indicator from the OSPAR candidate indicator Production of Phytoplankton' from the Department of the Environment, Fisheries and Rural Affairs (DEFRA) (Contract No.C7772). A European Regional Development Fund through the INTERREG VA France-Channel-England program called 'Sentinel-3 products for detecting Eutrophication and Harmful Algal Bloom events' (Contract No.106 S3-EUROHAB). An EU Horizons 2020 contract called 'Strategies for Environmental Monitoring of Marine Carbon Capture and Storage (STEMM-CCS; contract no.654462) and Deutsche Forschungsgemeinschaft.

References

- Achterberg, E.P., Moore, C.M., Henson, S.A., Steigenberger, S., Stohl, A., Eckhardt, S., Avendano, L.C., Cassidy, M., Hembury, D., Klar, J.K., Lucas, M.L., Macey, A.L., Marsay, C.M., Ryan-Keogh, T.J., 2013. Natural iron fertilization by the Eyjafjallajökull volcanic eruption. *Geophys. Res. Lett.* 40, 921–926.
- Allen, J.R., Slinn, D.J., Shammon, T.M., Hartnoll, R.G., Hawkins, S.J., 1998. Evidence for eutrophication of the Irish Sea over four decades. *Limnol. Oceanogr.* 43, 1970–1974.
- Alvera-Azcarate, A., Van der Zande, D., Barth, A., Troupin, C., Martin, S., Beckers, J.M., 2021. Analysis of 23 years of daily cloud-free chlorophyll and suspended particulate matter in the Greater North Sea. *Front. Mar. Sci.* 8.
- Antoine, D., Andre, J.M., Morel, A., 1996. Oceanic primary production. 2. Estimation at global scale from satellite (coastal zone color scanner) chlorophyll. *Glob. Biogeochem. Cycles* 10, 57–69.
- Arabi, B., Salama, M.S., Pitarch, J., Verhoef, W., 2020. Integration of in-situ and multi-sensor satellite observations for long-term water quality monitoring in coastal areas. *Remote Sens. Environ.* 239.
- Barnes, M.K., Tilstone, G.H., Suggett, D.J., Widdicombe, C.E., Bruun, J., Martinez-Vicente, V., Smyth, T.J., 2015. Temporal variability in total, micro- and nano-phytoplankton primary production at a coastal site in the Western English Channel. *Prog. Oceanogr.* 137, 470–483.

- Battye, W., Aneja, V.P., Schlesinger, W.H., 2017. Is nitrogen the next carbon? *Earths Future* 5, 894–904.
- Beaugrand, G., 2004. The North Sea regime shift: evidence, causes, mechanisms and consequences. *Prog. Oceanogr.* 60, 245–262.
- Becker, K.W., Harke, M.J., Mende, D.R., Muratore, D., Weitz, J.S., DeLong, E.F., Dyhman, S.T., Van Mooy, B.A.S., 2021. Combined pigment and metatranscriptomic analysis reveals highly synchronized diel patterns of phenotypic light response across domains in the open oligotrophic ocean. *ISME J.* 15, 520–533.
- Behrenfeld, M.J., O'Malley, R.T., Siegel, D.A., McClain, C.R., Sarmiento, J.L., Feldman, G.C., Milligan, A.J., Falkowski, P.G., Letelier, R.M., Boss, E.S., 2006. Climate-driven trends in contemporary ocean productivity. *Nature* 444, 752–755.
- van Beusekom, J.E.E., Carstensen, J., Dolch, T., Grage, A., Hofmeister, R., Lenhart, H., Kerimoglu, O., Kolbe, K., Patsch, J., Rick, J., Ronn, L., Ruiter, H., 2019. Wadden sea eutrophication: long-term trends and regional differences. *Front. Mar. Sci.* 6.
- Blondeau-Patissier, D., Gower, J.F.R., Dekker, A.G., Phinn, S.R., Brando, V.E., 2014. A review of ocean color remote sensing methods and statistical techniques for the detection, mapping and analysis of phytoplankton blooms in coastal and open oceans. *Prog. Oceanogr.* 123, 123–144.
- Boalch, G.T., 1987. Changes in the phytoplankton of the western English Channel in recent years. *Br. Phycol. J.* 22, 225–235.
- Boalch, G.T., Harbour, D.S., Butler, E.I., 1978. Seasonal phytoplankton production in the western English Channel 1964–1974. *J. Mar. Biol. Assoc. U. K.* 58, 943–953.
- Bopp, L., Monfray, P., Aumont, O., Dufresne, J.L., Le Treut, H., Madec, G., Terray, L., Orr, J.C., 2001. Potential impact of climate change on marine export production. *Glob. Biogeochem. Cycles* 15, 81–99.
- Boyd, P.W., Jickells, T., Law, C.S., Blain, S., Boyle, E.A., Buesseler, K.O., Coale, K.H., Cullen, J.J., de Baar, H.J.W., Follows, M., Harvey, M., Lancelot, C., Levasseur, M., Owens, N.P.J., Pollard, R., Rivkin, R.B., Sarmiento, J., Schoemann, V., Smetacek, V., Takeda, S., Tsuda, A., Turner, S., Watson, A.J., 2007. Mesoscale iron enrichment experiments 1993–2005: synthesis and future directions. *Science* 315, 612–617.
- Boynton, W.R., Ceballos, M.A.C., Bailey, E.M., Hodgkins, C.L.S., Humphrey, J.L., Testa, J.M., 2018. Oxygen and nutrient exchanges at the sediment-water interface: a global synthesis and critique of estuarine and coastal data. *Estuar. Coasts* 41, 301–333.
- Brito, A.C., Brotas, V., Caetano, M., Coutinho, T.P., Bordalo, A.A., Icelly, J., Neto, J.M., Serodio, J., Moita, T., 2012. Defining phytoplankton class boundaries in Portuguese transitional waters: an evaluation of the ecological quality status according to the Water Framework Directive. *Ecol. Indic.* 19, 5–14.
- Cadee, G.C., Hegeman, J., 2002. Phytoplankton in the Marsdiep at the end of the 20th century: 30 years monitoring biomass, primary production, and Phaeocystis blooms. *J. Sea Res.* 48, 97–110.
- Capuzzo, E., Lynam, C.P., Barry, J., Stephens, D., Forster, R.M., Greenwood, N., McQuatters-Gollop, A., Silva, T., van Leeuwen, S.M., Engelhard, G.H., 2018. A decline in primary production in the North Sea over 25 years, associated with reductions in zooplankton abundance and fish stock recruitment. *Glob. Chang. Biol.* 24, E352–E364.
- Carr, M.E., Friedrichs, M.A.M., Schmeltz, M., Aita, M.N., Antoine, D., Arrigo, K.R., Asanuma, I., Aumont, O., Barber, R., Behrenfeld, M., Bidigare, R., Buitenhuis, E.T., Campbell, J., Ciotti, A., Dierssen, H., Dowell, M., Dunne, J., Esaias, W., Gentili, B., Gregg, W., Groom, S., Hoepffner, N., Ishizaka, J., Kameda, T., Le Quere, C., Lohrenz, S., Marra, J., Melin, F., Moore, K., Morel, A., Reddy, T.E., Ryan, J., Scardi, M., Smyth, T., Turpie, K., Tilstone, G., Waters, K., Yamanaka, Y., 2006. A comparison of global estimates of marine primary production from ocean color. *Deep-Sea Res. II Top. Stud. Oceanogr.* 53, 741–770.
- Chang, N.B., Imen, S., Vannah, B., 2015. Remote sensing for monitoring surface water quality status and ecosystem state in relation to the nutrient cycle: a 40-year perspective. *Crit. Rev. Environ. Sci. Technol.* 45, 101–166.
- Cloern, J.E., 2001. Our evolving conceptual model of the coastal eutrophication problem. *Mar. Ecol. Prog. Ser.* 210, 223–253.
- Cloern, J.E., Foster, S.Q., Kleckner, A.E., 2014. Phytoplankton primary production in the world's estuarine-coastal ecosystems. *Biogeosciences* 11, 2477–2501.
- Cole, H.S., Henson, S., Martin, A.P., Yool, A., 2015. Basin-wide mechanisms for spring bloom initiation: how typical is the North Atlantic? *ICES J. Mar. Sci.* 72, 2029–2040.
- Commission, E.U., 2000. Establishing a framework for Community action in the field of water policy (2000/60/EC). *Off. J. Eur. Community L327*, 1–72.
- Commission, E.U., 2008. Commission Decision 2008/915/EC. *Off. J. Eur. Community L332*, 20–44.
- Cristina, S., Icelly, J., Goela, P.C., DelValles, T.A., Newton, A., 2015. Using remote sensing as a support to the implementation of the European Marine Strategy Framework Directive in SW Portugal. *Cont. Shelf Res.* 108, 169–177.
- Desmit, X., Nohe, A., Borges, A.V., Prins, T., De Cauwer, K., Lagring, R., Van der Zande, D., Sabbe, K., 2020. Changes in chlorophyll concentration and phenology in the North Sea in relation to de-eutrophication and sea surface warming. *Limnol. Oceanogr.* 65, 828–847.
- Devlin, M., Painting, S., Best, M., 2007. Setting nutrient thresholds to support an ecological assessment based on nutrient enrichment, potential primary production and undesirable disturbance. *Mar. Pollut. Bull.* 55, 65–73.
- Doney, S.C., 2006. Oceanography - plankton in a warmer world. *Nature* 444, 695–696.
- Dugdale, R.C., Goering, J.J., 1967. Uptake of new and regenerated forms of nitrogen in primary productivity. *Limnol. Oceanogr.* 12, 196–206.
- Edwards, V., Icelly, J., Newton, A., Webster, R., 2005. The yield of chlorophyll from nitrogen: a comparison between the shallow Ria Formosa lagoon and the deep oceanic conditions at Sagres along the southern coast of Portugal. *Estuar. Coast. Shelf Sci.* 62, 391–403.
- Eliassen, S.K., Hatun, H., Larsen, K.M.H., Hansen, B., Rasmussen, T.A.S., 2017. Phenologically distinct phytoplankton regions on the Faroe Shelf-identified by satellite data, in-situ observations and model. *J. Mar. Syst.* 169, 99–110.
- Friedland, K.D., Mouw, C.B., Asch, R.G., Ferreira, A.S.A., Henson, S., Hyde, K.J.W., Morse, R.E., Thomas, A.C., Brady, D.C., 2018. Phenology and time series trends of the dominant seasonal phytoplankton bloom across global scales. *Glob. Ecol. Biogeogr.* 27, 551–569.
- Friedrichs, M.A.M., Carr, M.-E., Barber, R.T., Scardi, M., Antoine, D., Armstrong, R.A., Asanuma, I., Behrenfeld, M.J., Buitenhuis, E.T., Chai, F., Christian, J.R., Ciotti, A.M., Doney, S.C., Dowell, M., Dunne, J., Gentili, B., Gregg, W., Hoepffner, N., Ishizaka, J., Kameda, T., Lima, I., Marra, J., Melin, F., Moore, J.K., Morel, A., O'Malley, R.T., O'Reilly, J., Saba, V.S., Schmeltz, M., Smyth, T.J., Tjiputra, J., Waters, K., Westberry, T.K., Winguth, A., 2009. Assessing the uncertainties of model estimates of primary productivity in the tropical Pacific Ocean. *J. Mar. Syst.* 76, 113–133.
- Garcia-Garcia, L.M., Sivyver, D., Devlin, M., Painting, S., Collingridge, K., van der Molen, J., 2019. Optimizing monitoring programs: a case study based on the OSPAR eutrophication assessment for UK waters. *Front. Mar. Sci.* 5.
- Gohin, F., 2011. Annual cycles of chlorophyll-a, non-algal suspended particulate matter, and turbidity observed from space and in-situ in coastal waters. *Ocean Sci.* 7, 705–732.
- Gohin, F., Druon, J.N., Lampert, L., 2002. A five channel chlorophyll concentration algorithm applied to SeaWiFS data processed by SeaDAS in coastal waters. *Int. J. Remote Sens.* 23, 1639–1661.
- Gohin, F., Saulquin, B., Oger-Jeanneret, H., Lozac'h, L., Lampert, L., Lefebvre, A., Riou, P., Bruchon, F., 2008. Towards a better assessment of the ecological status of coastal waters using satellite-derived chlorophyll-a concentrations. *Remote Sens. Environ.* 112, 3329–3340.
- Gohin, F., Van der Zande, D., Tilstone, G., Eleveld, M.A., Lefebvre, M., Andrieux-Loyer, F., Blauw, A.N., Bryere, P., Devreker, D., Gamesson, P., Farinas, T.H., Lamaury, Y., Lampert, L., Lavigne, H., Menet-Nedelec, F., Pardo, S., Saulquin, B., 2019. Twenty years of satellite and in situ observations of surface chlorophyll-a from the northern Bay of Biscay to the eastern English Channel. Is the water quality improving? *Remote Sens. Environ.* 233.
- Grosse, F., Kreis, M., Lenhart, H.J., Patsch, J., Pohlmann, T., 2017. A novel modeling approach to quantify the influence of nitrogen inputs on the oxygen dynamics of the North Sea. *Front. Mar. Sci.* 4.
- Hallegraef, G.M., 2010. Ocean climate change, phytoplankton community responses, and harmful algal blooms: a formidable predictive challenge. *J. Phycol.* 46, 220–235.
- Harvey, E.T., Kratzer, S., Philipson, P., 2015. Satellite-based water quality monitoring for improved spatial and temporal retrieval of chlorophyll-a in coastal waters. *Remote Sens. Environ.* 158, 417–430.
- Henson, S.A., Robinson, I., Allen, J.T., Wanick, J.J., 2006. Effect of meteorological conditions on interannual variability in timing and magnitude of the spring bloom in the Irminger Basin, North Atlantic. *Deep-Sea Res. I Oceanogr. Res. Pap.* 53, 1601–1615.
- Henson, S.A., Dunne, J.P., Sarmiento, J.L., 2009. Decadal variability in North Atlantic phytoplankton blooms. *J. Geophys. Res. Oceans* 114.
- Howarth, R.W., Chan, F., Swaney, D.P., Marino, R.M., Hayn, M., 2021. Role of external inputs of nutrients to aquatic ecosystems in determining prevalence of nitrogen vs. phosphorus limitation of net primary productivity. *Biogeochemistry* 154, 293–306.
- Hu, C.M., Lee, Z., Franz, B., 2012. Chlorophyll a algorithms for oligotrophic oceans: a novel approach based on three-band reflectance difference. *J. Geophys. Res. Oceans* 117.
- de Jonge, V.N., Elliott, M., Orive, E., 2002. Causes, historical development, effects and future challenges of a common environmental problem: eutrophication. *Hydrobiologia* 475, 1–19.
- Kerimoglu, O., Voynova, Y.G., Chegini, F., Brix, H., Callies, U., Hofmeister, R., Klingbeil, K., Schrum, C., van Beusekom, J.E.E., 2020. Interactive impacts of meteorological and hydrological conditions on the physical and biogeochemical structure of a coastal system. *Biogeosciences* 17, 5097–5127.
- Koertzing, A., Send, U., Lampitt, R.S., Hartman, S., Wallace, D.W.R., Karstensen, J., Villagarcia, M.G., Llinas, O., DeGrandpre, M.D., 2008. The seasonal pCO₂ cycle at 49 degrees N/16.5 degrees W in the northeastern Atlantic Ocean and what it tells us about biological productivity. *J. Geophys. Res. Oceans* 113.
- Krug, L.A., Platt, T., Sathyendranath, S., Barbosa, A.B., 2018. Patterns and drivers of phytoplankton phenology off SW Iberia: a phenoregion based perspective. *Prog. Oceanogr.* 165, 233–256.
- Lapucci, C., Rella, M.A., Brandini, C., Ganzin, N., Gozzini, B., Maselli, F., Massi, L., Nuccio, C., Ortolani, A., Trees, C., 2012. Evaluation of empirical and semi-analytical chlorophyll algorithms in the Ligurian and North Tyrrhenian Seas. *J. Appl. Remote Sens.* 6.
- Lavigne, H., Van der Zande, D., Ruddick, K., Dos Santos, J.F.C., Gohin, F., Brotas, V., Kratzer, S., 2021. Quality-control tests for OC4, OC5 and NIR-red satellite chlorophyll-a algorithms applied to coastal waters. *Remote Sens. Environ.* 255.
- Lehmusluoto, P.O., Pesonen, L., 1973. Eutrophication in Helsinki and Espoo Sea areas measured as phytoplankton primary production. *Oikos* 202–208.
- Loisel, H., Vantrepotte, V., Ouillon, S., Ngoc, D.D., Herrmann, M., Tran, V., Meriaux, X., Dessailly, D., Jamet, C., Duhaut, T., Nguyen, H.H., Nguyen, T.V., 2017. Assessment and analysis of the chlorophyll-a concentration variability over the Vietnamese coastal waters from the MERIS ocean color sensor (2002–2012). *Remote Sens. Environ.* 190, 217–232.
- Lomas, M.W., Steinberg, D.K., Dickey, T., Carlson, C.A., Nelson, N.B., Condon, R.H., Bates, N.R., 2010. Increased ocean carbon export in the Sargasso Sea linked to climate variability is countered by its enhanced mesopelagic attenuation. *Biogeosciences* 7, 57–70.
- Longhurst, A., Sathyendranath, S., Platt, T., Caverhill, C., 1995. An estimate of global primary production in the ocean from satellite radiometer data. *J. Plankton Res.* 17, 1245–1271.
- Loureiro, S., Newton, A., Icelly, J., 2005. Effects of nutrient enrichments on primary production in the Ria Formosa coastal lagoon (Southern Portugal). *Hydrobiologia* 550, 29–45.
- Marshak, A.R., Link, J.S., 2021. Primary production ultimately limits fisheries economic performance. *Sci. Rep.* 11.
- McQuatters-Gollop, A., Reid, P.C., Edwards, M., Burkill, P.H., Castellani, C., Batten, S., Gieskes, W., Beare, D., Bidigare, R.R., Head, E., Johnson, R., Kahru, M., Koslow, J.A., Pena, A., 2011. Is there a decline in marine phytoplankton? *Nature* 472, E6–E7.
- Melin, F., Vantrepotte, V., Chuprin, A., Grant, M., Jackson, T., Sathyendranath, S., 2017. Assessing the fitness-for-purpose of satellite multi-mission ocean color climate data records: a protocol applied to OC-CCI chlorophyll-a data. *Remote Sens. Environ.* 203, 139–151.
- Morel, A., 1991. Light and marine photosynthesis - a spectral model with geochemical and climatological implications. *Prog. Oceanogr.* 26, 263–306.

- Morel, A., Prieur, L., 1977. Analysis of variations in ocean color. *Limnol. Oceanogr.* 22, 709–722.
- Naustvoll, L.J., Melle, W., Klevjer, T., Drinkwater, K.F., Strand, E., Knutsen, T., 2020. Dynamics of phytoplankton species composition, biomass and nutrients in the North Atlantic during spring and summer - a trans-Atlantic study. *Deep-Sea Res. II Top. Stud. Oceanogr.* 180.
- Nixon, S.W., 1995. Coastal marine eutrophication - a definition, social causes, and future concerns. *Ophelia* 41, 199–219.
- Novoa, S., Chust, G., Sagaminaga, Y., Revilla, M., Borja, A., Franco, J., 2012. Water quality assessment using satellite-derived chlorophyll-a within the European directives, in the southeastern Bay of Biscay. *Mar. Pollut. Bull.* 64, 739–750.
- Ornoldsdottir, E.B., Lumsden, S.E., Pinckney, J.L., 2004. Phytoplankton community growth-rate response to nutrient pulses in a shallow turbid estuary, Galveston Bay, Texas. *J. Plankton Res.* 26, 325–339.
- OSPAR, 2003. In: Series, E. (Ed.), *OSPAR Integrated Report 2003 on the Eutrophication Status of the OSPAR Maritime Area*. OSPAR, Oslo-Paris, p. 59.
- OSPAR, 2017. *Eutrophication status of the OSPAR maritime area. Third Integrated Report on the Eutrophication Status of the OSPAR Maritime Area*. Oslo-Paris Commission.
- Rabalais, N.N., Turner, R.E., Diaz, R.J., Justic, D., 2009. Global change and eutrophication of coastal waters. *ICES J. Mar. Sci.* 66, 1528–1537.
- Racault, M.F., Le Quere, C., Buitenhuis, E., Sathyendranath, S., Platt, T., 2012. Phytoplankton phenology in the global ocean. *Ecol. Indic.* 14, 152–163.
- Reid, P.C., Taylor, A.H., Stephens, J.A., 1988. *The Hydrography and Hydrographic Balances of the North Sea*. Springer-Verlag, Berlin, Heidelberg, New York, London, Paris, Tokyo.
- Reid, P.C., Borges, M.D., Svendsen, E., 2001a. A regime shift in the North Sea circa 1988 linked to changes in the North Sea horse mackerel fishery. *Fish. Res.* 50, 163–171.
- Reid, P.C., Holliday, N.P., Smyth, T.J., 2001b. Pulses in the eastern margin current and warmer water off the north west European shelf linked to North Sea ecosystem changes. *Mar. Ecol.-Prog. Ser.* 215, 283–287.
- Ryther, J.H., Dunstan, W.M., 1971. Nitrogen, phosphorus, and eutrophication in coastal marine environment. *Science* 171, 1008.
- Saba, V.S., Friedrichs, M.A.M., Antoine, D., Armstrong, R.A., Asanuma, I., Behrenfeld, M.J., Ciotti, A.M., Dowell, M., Hoepfner, N., Hyde, K.J.W., Ishizaka, J., Kameda, T., Marra, J., Melin, F., Morel, A., O'Reilly, J., Scardi, M., Smith Jr., W.O., Smyth, T.J., Tang, S., Uitz, J., Waters, K., Westberry, T.K., 2011. An evaluation of ocean color model estimates of marine primary productivity in coastal and pelagic regions across the globe. *Biogeosciences* 8, 489–503.
- Sarang, R.K., 2011. Remote sensing of chlorophyll and sea surface temperature in Indian water with impact of 2004 Sumatra Tsunami. *Mar. Geod.* 34, 152–166.
- Sarmiento, J.L., Slater, R., Barber, R., Bopp, L., Doney, S.C., Hirst, A.C., Kleypas, J., Matear, R., Mikolajewicz, U., Monfray, P., Soldatov, V., Spall, S.A., Stouffer, R., 2004. Response of ocean ecosystems to climate warming. *Glob. Biogeochem. Cycles* 18.
- Sathyendranath, S., Brewin, R.J.W., Brockmann, C., Brotas, V., Calton, B., Chuprin, A., Cipollini, P., Couto, A.B., Dingle, J., Doerffer, R., Donlon, C., Dowell, M., Farman, A., Grant, M., Groom, S., Horseman, A., Jackson, T., Krasemann, H., Lavender, S., Martinez-Vicente, V., Mazeran, C., Melin, F., Moore, T.S., Muller, D., Regner, P., Roy, S., Steele, C.J., Steinmetz, F., Swinton, J., Taberner, M., Thompson, A., Valente, A., Zuhlke, M., Brando, V.E., Feng, H., Feldman, G., Franz, B.A., Frouin, R., Gould, R.W., Hooker, S.B., Kahru, M., Kratzer, S., Mitchell, B.G., Muller-Karger, F.E., Sosik, H.M., Voss, K.J., Werdell, J., Platt, T., 2019. An ocean-colour time series for use in climate studies: the experience of the ocean-colour climate change initiative (OC-CCI). *Sensors* 19.
- Saulquin, B., Gohin, F., Garrello, R., 2011. Regional objective analysis for merging high-resolution MERIS, MODIS/Aqua, and SeaWiFS chlorophyll-a data from 1998 to 2008 on the European Atlantic shelf. *IEEE Trans. Geosci. Remote Sens.* 49, 143–154.
- Sava, E., Edwards, B., Cervone, G., 2014. Chlorophyll increases off the coasts of Japan after the 2011 tsunami using NASA/MODIS data. *Nat. Hazards Earth Syst. Sci.* 14, 1999–2008.
- Silva, E., Counillon, F., Brajard, J., Korosov, A., Pettersson, L.H., Samuelsen, A., Keenlyside, N., 2021. Twenty-one years of phytoplankton bloom phenology in the Barents, Norwegian, and North Seas. *Front. Mar. Sci.* 8.
- Smetacek, V., Zingone, A., 2013. Green and golden seaweed tides on the rise. *Nature* 504, 84–88.
- Smyth, T.J., Tilstone, G.H., Groom, S.B., 2005. Integration of radiative transfer into satellite models of ocean primary production. *J. Geophys. Res.* Oceans 110.
- Steinberg, D.K., Carlson, C.A., Bates, N.R., Johnson, R.J., Michaels, A.F., Knap, A.H., 2001. Overview of the US JGOFS Bermuda Atlantic Time-series Study (BATS): a decade-scale look at ocean biology and biogeochemistry. *Deep-Sea Res. II Top. Stud. Oceanogr.* 48, 1405–1447.
- Stock, C.A., Dunne, J.P., John, J.G., 2014. Drivers of trophic amplification of ocean productivity trends in a changing climate. *Biogeosciences* 11, 7125–7135.
- Sundermann, J., Pohlmann, T., 2011. A brief analysis of North Sea physics. *Oceanologia* 53, 663–689.
- Sverdrup, H.U., 1957. On conditions for the vernal blooming of phytoplankton. *J. Cons. Cons. Int. Explor. Mer.* 18, 287–295.
- Taboada, F.G., Anadon, R., 2014. Seasonality of North Atlantic phytoplankton from space: impact of environmental forcing on a changing phenology (1998–2012). *Glob. Chang. Biol.* 20, 698–712.
- Takahashi, T., Sutherland, S.C., Wanninkhof, R., Sweeney, C., Feely, R.A., Chipman, D.W., Hales, B., Friederich, G., Chavez, F., Sabine, C., Watson, A., Bakker, D.C.E., Schuster, U., Metzl, N., Yoshikawa-Inoue, H., Ishii, M., Midorikawa, T., Nojiri, Y., Koertzing, A., Steinhoff, T., Hoppema, M., Olafsson, J., Arnarson, T.S., Tilbrook, B., Johannessen, T., Olsen, A., Bellerby, R., Wong, C.S., Delille, B., Bates, N.R., de Baar, H.J.W., 2009. Climatological mean and decadal change in surface ocean pCO₂, and net sea-air CO₂ flux over the global oceans (vol 56, pg 554, 2009). *Deep-Sea Res. I Oceanogr. Res. Pap.* 56, 2075–2076.
- Tang, W.Y., Llort, J., Weis, J., Perron, M.M.G., Basart, S., Li, Z.C., Sathyendranath, S., Jackson, T., Rodriguez, E.S., Proemse, B.C., Bowie, A.R., Schallenberg, C., Strutton, P.G., Matear, R., Cassar, N., 2021. Widespread phytoplankton blooms triggered by 2019–2020 Australian wildfires. *Nature* 597, 370–+.
- Tett, P., Gowen, R., Mills, D., Fernandes, T., Gilpin, L., Huxham, M., Kennington, K., Read, P., Service, M., Wilkinson, M., Malcolm, S., 2007. Defining and detecting undesirable disturbance in the context of marine eutrophication. *Mar. Pollut. Bull.* 55, 282–297.
- Tilstone, G.H., Smyth, T.J., Gowen, R.J., Martinez-Vicente, V., Groom, S.B., 2005. Inherent optical properties of the Irish Sea and their effect on satellite primary production algorithms. *J. Plankton Res.* 27, 1127–1148.
- Tilstone, G., Smyth, T., Poulton, A., Hutson, R., 2009. Measured and remotely sensed estimates of primary production in the Atlantic Ocean from 1998 to 2005. *Deep-Sea Res. II Top. Stud. Oceanogr.* 56, 918–930.
- Tilstone, G.H., Angel-Benavides, I.M., Pradhan, Y., Shutler, J.D., Groom, S., Sathyendranath, S., 2011. An assessment of chlorophyll-a algorithms available for SeaWiFS in coastal and open areas of the Bay of Bengal and Arabian Sea. *Remote Sens. Environ.* 115, 2277–2291.
- Tilstone, G.H., Miller, P.I., Brewin, R.J.W., Priede, I.G., 2014. Enhancement of primary production in the North Atlantic outside of the spring bloom, identified by remote sensing of ocean colour and temperature. *Remote Sens. Environ.* 146, 77–86.
- Tilstone, G.H., Taylor, B.H., Blondeau-Patissier, D., Powell, T., Groom, S.B., Rees, A.P., Lucas, M.I., 2015. Comparison of new and primary production models using SeaWiFS data in contrasting hydrographic zones of the northern North Atlantic. *Remote Sens. Environ.* 156, 473–489.
- Tilstone, G., Mallor-Hoya, S., Gohin, F., Couto, A.B., Sa, C., Goela, P., Cristina, S., Ains, R., Icelly, J., Zuhlke, M., Groom, S., 2017. Which ocean colour algorithm for MERIS in North West European waters? *Remote Sens. Environ.* 189, 132–151.
- Tilstone, G.H., Pardo, S., Dall, G., Brewin, R.J.W., Nencioli, F., Dessailly, D., Kwiatkowska, E., Casal, T., Donlon, C., 2021. Performance of ocean colour chlorophyll a algorithms for Sentinel-3 OLCI, MODIS-Aqua and Suomi-VIIRS in open-ocean waters of the Atlantic. *Remote Sens. Environ.* 260.
- Wang, Y.T., Chen, H.H., Tang, R., He, D., Lee, Z.P., Xue, H.J., Wells, M., Boss, E., Chai, F., 2022. Australian fire nourishes ocean phytoplankton bloom. *Sci. Total Environ.* 807.
- Xie, Y.Y., Tilstone, G.H., Widdicombe, C., Woodward, E.M.S., Harris, C., Barnes, M.K., 2015. Effect of increases in temperature and nutrients on phytoplankton community structure and photosynthesis in the western English Channel. *Mar. Ecol. Prog. Ser.* 519, 61–73.
- Zhai, L., Gudmundsson, K., Miller, P., Peng, W., Gudfinnsson, H., Debes, H., Hatun, H., White III, G.N., Hernandez Walls, R., Sathyendranath, S., Platt, T., 2012. Phytoplankton phenology and production around Iceland and Faroes. *Cont. Shelf Res.* 37, 15–25.
- Zhai, L., Platt, T., Tang, C., Sathyendranath, S., Walne, A., 2013. The response of phytoplankton to climate variability associated with the North Atlantic Oscillation. *Deep-Sea Res. II Top. Stud. Oceanogr.* 93, 159–168.
- Zhang, H.R., Wang, Y.T., Xiu, P., Qi, Y.Q., Chai, F., 2021. Roles of iron limitation in phytoplankton dynamics in the western and eastern subarctic Pacific. *Front. Mar. Sci.* 8.